Developmental Biology 359 (2011) 110–123

Contents lists available at ScienceDirect

Developmental Biology

journal homepage: www.elsevier.com/developmentalbiology

Evolution of Developmental Control Mechanisms

Patterns of cell lineage, movement, and migration from germ layer specification to gastrulation in the amphipod crustacean *Parhyale hawaiensis*

Frederike Alwes [a], Billy Hinchen [a,b], Cassandra G. Extavour [a,*]

[a] Department of Organismic and Evolutionary Biology, Harvard University, 16 Divinity Avenue, Cambridge, MA 02138, USA
[b] Department of Zoology, University of Cambridge, Downing Street, Cambridge, Cambridgeshire, CB2 3EJ, England, UK

ARTICLE INFO

Article history:
Received for publication 21 May 2011
Revised 14 July 2011
Accepted 20 July 2011
Available online 28 July 2011

Keywords:
Cell lineage
Regulation
Crustacean
Gastrulation
Cleavage
Embryogenesis

ABSTRACT

The acquisition of specific cell fates throughout embryonic development is one of the core problems in developmental and evolutionary biology. In the amphipod *Parhyale hawaiensis* all three germ layers and the germ line are determined by the eight-cell stage. Despite this early fate determination, multiple cell types can be replaced following ablation of their founder cells, showing that this embryo also has significant regulative properties. Here we present a cellular-level resolution lineage analysis for *P. hawaiensis* embryos between fertilization and gastrulation, including analysis of cleavage patterns, division times, and clonal behaviors. We compare these cellular behaviors in wild type embryos with those in embryos where specific founder cells have been ablated, or where zygotic transcription has been inhibited. We observe that when germ line, endoderm or mesoderm founder cells are ablated, the remaining cells do not alter their cleavage or migration behaviors before the onset of gastrulation. In the absence of zygotic transcription, ingression movements proceed normally, but epibolic movements are disrupted. This indicates that the embryo's regulative response to germ layer founder loss, in the form of altered cell behavior, is realized in the ~32 h between gastrulation and early germ band elongation, and is likely to require zygotic reprogramming rather than alternative deployment of maternally supplied determinants. Combining these data with the observations of previous studies, we propose a framework to elucidate the molecular mechanisms that regulate the determinative and regulative properties of the *P. hawaiensis* embryo.

Introduction

Animal development requires the correct specification, differentiation and interaction of multiple cell types. In most metazoans gastrulation establishes three germ layers, ectoderm, mesoderm, and endoderm. The timing of this process and the extent to which cells are irreversibly differentiated, however, vary between species and between different cell types. For example, in mice (Conlon and Beddington, 1995; Tam et al., 1993), zebrafish (Yin et al., 2009) and *Drosophila* (Leptin and Grunewald, 1990), gastrulation begins after the blastoderm stage, when large numbers of cells are available to participate in the process and acquire their germ layer fates largely by virtue of gastrulation. However, in nematodes (Deppe et al., 1978; Sulston et al., 1983), ascidians (Conklin, 1905; Nishida and Satoh, 1983), and spirally cleaving gastropods (Dictus and Damen, 1997; van den Biggelaar et al., 1997), germ layer fates are determined and specified through cell lineage relationships prior to gastrulation processes.

Among the arthropods, gastrulation has been most intensively studied in the fruit fly *Drosophila melanogaster* (reviewed in Leptin, 1999). In this fly, maternal factors operate during early syncytial cleavages to confer mesodermal fate on a field of several hundred cells, which collectively undergo complex gastrulation movements (see for example McMahon et al., 2010). While some gastrulation movements can take place in the absence of mesoderm (Ip et al., 1994), lost mesoderm cannot be replaced later in development (Simpson, 1983). However, much less is known about the linkage between the mechanisms of cell lineage, germ layer determination and gastrulation in arthropods that gastrulate with a small number of cells.

The amphipod crustacean *Parhyale hawaiensis* is a promising laboratory model organism increasingly used for comparative arthropod development and evolution studies (Rehm et al., 2008). *In vivo* labeling experiments have led to a fate map showing that the future body axes, the three germ layers, and the germ line are already established as early as the eight-cell stage, which comprises four macromeres and four micromeres (Gerberding et al., 2002) (Fig. 1A). Three of the macromeres (**Ep**, **El**, **Er**) give rise to ectodermal tissue and one (**Mav**) gives rise to the anterior and visceral mesoderm. Two of the micromeres (**ml** and **mr**) give rise to the trunk mesoderm, one (**en**) is described to give rise to the endoderm and one micromere (**g**) constitutes the germ line (Gerberding et al., 2002). **g** receives its germ line fate through a cytoplasmic determinant that is asymmetrically

* Corresponding author. Fax: +1 617 496 9507.
E-mail address: extavour@oeb.harvard.edu.

0012-1606/$ – see front matter © 2011 Elsevier Inc. All rights reserved.
doi:10.1016/j.ydbio.2011.07.029

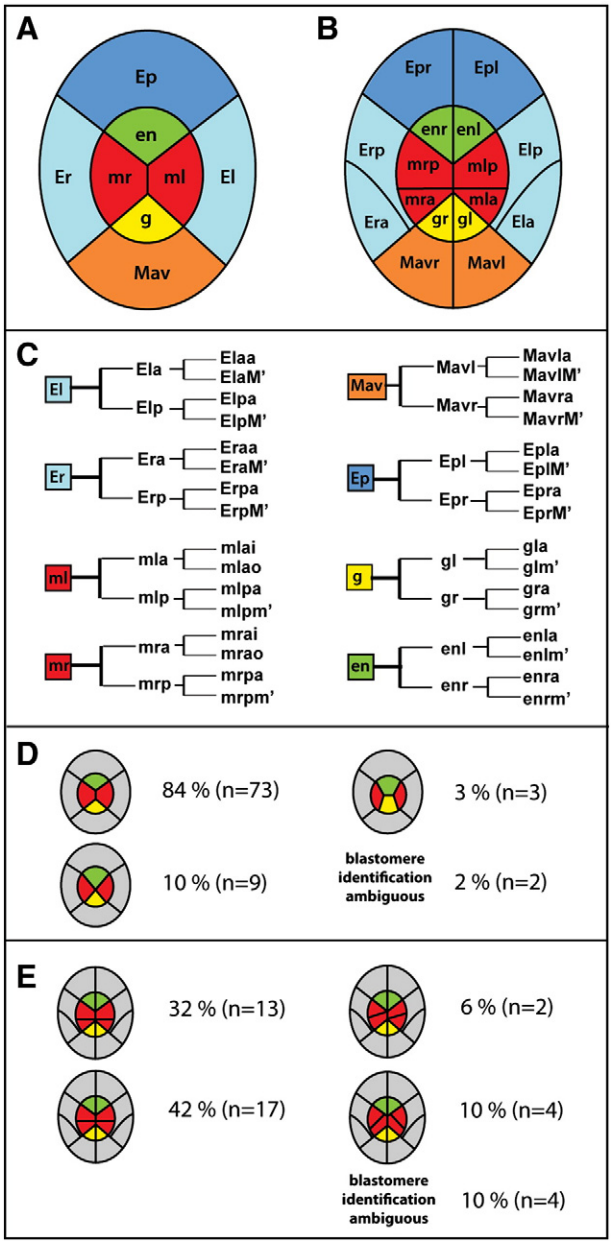

Fig. 1. Schematic of early cell nomenclature and cellular arrangements in *P. hawaiensis*. (A) Eight-cell stage. The blastomeres are designated according to Gerberding et al. (2002), providing the basis for the nomenclature for their descendants in the following division cycles. (B) 16-cell stage. Fourth cleavage blastomeres are individually distinguished by lower case letters according to their relative position: left (**l**) or right (**r**) for descendants of **Mav**, **g**, **en** or **Ep**, and anterior (**a**) or posterior (**p**) for descendants of **ml**, **mr**, **El** and **Er**. (C) Nomenclature of the fourth and fifth cleavage blastomeres. At fifth cleavage, macromere descendants are distinguished by relative position as anterior (**a**) or towards the macromeres (**M′**), while **g**, **en**, **mrp** and **mlp** descendants are distinguished as being anterior (**a**) or towards the micromeres (**m′**). We use apostrophes in the suffix of the fifth cleavage blastomere names to distinguish the letter "m" here from its use in the names of the third cleavage blastomeres. The descendants of **mra** and **mla** that sink below the surface of the yolk shortly following fifth cleavage are designated as inner (**i**), while those that remain visible on the surface of the yolk are designated as outer (**o**). (D)–(E) The arrangement of micromeres at eight- and 16-cell stages can diverge from the arrangement shown in A and B. (D) At the eight-cell stage in most cases (84%) the **m** micromeres are adjacent to each other and share a cell border, whereas **g** and **en** do not. In some cases (10%) the micromeres are arranged so that they are all in contact with each other and in a few cases (3%) **g** is in contact with **en**. In a small percentage (2%) of eggs the blastomeres cannot be unambiguously identified (n = 87). (E) In the most common arrangement at the 16-cell stage (74%) all mesoderm micromeres are in direct contact with their left/right counterpart. In a minority of cases (16%) only one of these two left/right pairs are in contact. In 10% of embryos the identity of blastomeres is ambiguous (n = 40).

segregated as early as first cleavage, and loss of **g** at the eight-cell stage results in hatchlings lacking germ cells, consistent with early determination of this cell fate (Extavour, 2005). In contrast, if up to two of the mesoderm precursor cells (**Mav**, **mr** or **ml**) are ablated at the eight-cell stage, the remaining mesoderm precursor is able to replace the lost cells, resulting in hatchlings with normal mesoderm (Price et al., 2010). However, no other cell type (ectoderm, endoderm or germ line) has the capacity to regulatively generate mesoderm tissue during embryogenesis (Price et al., 2010).

Gastrulation and germ band formation in *P. hawaiensis* principally involves large scale cell migrations and cellular movements that include the reorganization of the two tiered germ layer precursors at the eight-cell stage, into the bilaterally symmetrical germ disk stage of the later embryo (Gerberding et al., 2002; Price, 2005; Price and Patel, 2008). However, several aspects of *P. hawaiensis* gastrulation remain to be clarified, particularly in light of the regulative capacity of the embryo to replace lost mesoderm precursors (Price et al., 2010). Some outstanding questions include, how invariant are the lineage patterns and migratory trajectories of each germ layer lineage? Does lineage identity or positional information determine cellular behavior leading up to and during gastrulation? Are these behaviors cell-autonomous and maternally determined, or do they rely on signals from neighboring cells and zygotic gene regulation? Is the lineage of those cells that initiate gastrulation invariant? How do cell behaviors change when germ layer precursors are removed?

The best studied animal where these questions have been answered for an embryo with similarly early determined cell fate development is the nematode *Caenorrhabditis elegans* (Sulston et al., 1983). In addition to genetic analysis, physical and pharmacological manipulations (reviewed by Nance et al., 2005), 4D microscopy-assisted cell lineage analysis (Schnabel et al., 1997) is a powerful technique to improve our understanding of wild type processes (see for example Bischoff and Schnabel, 2006; Bischoff et al., 2008; Tassy et al., 2006).

In this study, we used live imaging and 4D microscopy in conjunction with the cell lineage analysis software SIMI° BioCell (Schnabel et al., 1997) to analyze *P. hawaiensis* embryogenesis from early cleavage to early germ disk stages at cellular level detail. We traced the cell lineages, behaviors, and clonal compositions involved in cell movement and gastrulation. We determined the extent of regular and required cell contacts and maternal/zygotic regulation, and compared wild type embryos with micromere-ablated embryos in these respects. We discuss our findings in the context of the cell lineage and regulatory properties of other arthropod embryonic cell types.

Materials and methods

Animal culture and embryo collection

P. hawaiensis was cultured in covered plastic tanks with a crushed coral (Instant) substrate and artificial seawater (ASW, specific gravity 1.019–1.022, Tropic Marin) oxygenated with air stones at 28–30 °C. Animals were fed daily with ground aquaculture feed (40% TetraPond® wheat germ sticks, 40% TetraMin® flake food, and 20% Tropical® spirulina). Eggs were collected as described in Rehm et al. (2008) and kept in filtered (0.45 μm filter) ASW (FASW; specific gravity 1.019) containing Penicillin–Streptomycin (Cellgro) 1:100 (stock solution 10,000 U/ml penicillin, 10,000 μg/ml streptomycin), Fungizone-Amphotericin B (Fulka) 1:40, pH 8.15 (stock solution 100 μg/ml).

4D microscopy

The general principle and application of 4D-microscopy as a multiple focal plane time-lapse recording method are described in detail by Schnabel et al. (1997) and Hejnol and Schnabel (2006). For this study we

used a Zeiss AxioImager Z1 connected to an AxioCam MRm camera. Embryos at the eight-cell stage were mounted in FASW on glass microscope slides. The cover slip margins were sealed with Vaseline or vacuum grease to prevent evaporation of the FASW, thus avoiding changes in salinity.

The recordings were captured with AxioVision 4.6 at a constant temperature of 25 °C. For each experiment, between 30 and 45 focal planes were captured with a combination of white incident fiber optic light and Nomarski optics every 5 min with ~4 µm distance between focal planes. After recordings had finished embryos used for the cell lineage analysis were transferred to 12-place multi-well dishes with FASW and cultured at 25 °C until hatching. All analyses of wild type cell lineage used only recordings of embryos that (a) could be cultured to normal viable juveniles; and (b) were recorded in an orientation allowing for the most informative tracing of cellular processes leading up to gastrulation. Table 1 summarizes the duration of the recordings and the respective cell lineages that were followed in each experiment. A subset of embryos was recorded until the rosette stage or through gastrulation and subsequently fixed for 15–20 min in 3.7% in formaldehyde PBS (1.86 mM NaH_2PO_4; 8.41 mM Na_2HPO_4; 0.175 M NaCl; pH 7.2) and stored in absolute methanol for antibody staining.

Exported TIFF files of the recordings were renamed using the free software AntRenamer 2.1 to provide a format readable by SIMI°-BioCell. Cell lineages were then analyzed using SIMI°BioCell 4.0.153 (SIMI°Reality Motion Systems GmbH, Unterschleissheim, Germany).

Image analysis

Figures and schematics were created with Adobe Photoshop CS4 and Adobe Illustrator CS4. Original images of focal stacks were rendered using Helicon Focus 5.1. Captions and colorations in movies were created using Windows Movie Maker, Adobe Premiere and Adobe After Effects. Screenshot movies were captured by VRtainment CapturePad.

Antibody staining

Embryos fixed for antibody staining and stored in methanol as described above were washed in PBS over night. The antibody staining procedure followed standard protocols (Patel, 1994) with slight modifications. Washing after primary antibody incubation was performed with the addition of 5% DMSO to the PBT buffer. Washing steps were prolonged and increased in number compared to Patel et al. (1989). Blocking before incubation in primary and secondary antibodies was performed in PBT + N (1× PBS, 2% BSA, 1% Triton X-100, 5% DMSO, 5% normal goat serum (NGS)) for 30 min. After staining and washing embryos were washed again in PBT + 5% DMSO and mounted in 70% PBS-Glycerol. Primary antibodies were mouse anti-acetylated tubulin (Sigma T6793) 1:100, anti-α-tubulin (Sigma F2168, clone DMIA) 1:50, and rabbit anti-ß-catenin (Sigma C2206) 1:50. Secondary antibodies were goat anti-mouse Alexa 488 and goat anti-rabbit Alexa 647 (Invitrogen) 1:200 or 1:500. Phalloidin-Alexa 555 conjugate (Invitrogen) was used at 1:50.

Table 1
Recordings of wild type embryos used for cell lineage analysis. Summary of the time length of all recordings (hh:min) analyzed in this study. Time values shown refer only to the duration of the recording; all 17 embryos considered here were successfully raised until hatching (~10 days at 25 °C). The recordings start at the eight-cell stage and extend to at least the rosette stage, except for the recording of embryo # 05. Black dots indicate which blastomeres had their cell lineages traced in each movie.

# embryo recorded	Duration of recording (hh:min)	Blastomere traceable in recording							
		g	**Mav**	**ml**	**El**	**mr**	**Er**	**en**	**Ep**
# 01	17:00	•	•	•	•	•	•	•	
# 02	21:00	•		•		•		•	
# 03	19:55	•	•	•	•				
# 04	19:55	•	•	•	•	•	•		
# 05	6:00	•	•	•	•	•	•		
# 06	17:04	•	•	•		•			
# 07	19:55	•	•		•		•		
# 08	14:40	•	•			•	•		
# 09	23:30	•	•			•	•		
# 10	16:35	•	•						
# 11	15:31	•	•			•	•		
# 12	15:31	•	•	•	•		•		
# 13	9:35	•	•						
# 14	16:05	•	•	•	•	•	•	•	
# 15	8:55		•		•		•		•
# 16	21:20			•	•	•	•	•	•
# 17	21:20	•	•	•	•	•	•	•	

Blastomere ablations

Manual ablation was performed on embryos that had just completed third cleavage. We performed manual ablation rather than photoablation or DNAse/RNAse injection as has been previously described (Price et al., 2010), in order to completely remove all cell content from eggs. Embryos were transferred onto a silicone plate (Sylgard 184) in a droplet of FASW and positioned under a dissection microscope. Only eggs in which **g** could be clearly identified as the smallest micromere and as the sister cell of the smallest macromere **Mav** were used for the ablations. A hole was poked into the targeted cell using sharpened tungsten needles, and a mouth pipette was used to remove all cell contents. Ablated embryos were then recorded for cell lineage analysis, and raised through subsequent embryogenesis.

Pharmacological inhibition of transcription

Embryos were incubated in FASW containing alpha-amanitin (Sigma Cat. No. A2263; stock solution made up in DMSO) at a final concentration of 25 or 50 µg/ml; these concentrations completely abolish transcription by RNA Polymerase II in *Mus musculus* (Liu et al., 2004) and *Xenopus laevis* (Newport and Kirschner, 1982); results were not significantly different between the two concentrations and were pooled for analysis. Control embryos were incubated in equivalent final concentrations of DMSO; results were not significantly different across concentrations and were pooled for analysis. Incubation was continuous from the one, two or four-cell stages for at least 24 h; results were not significantly different between initial incubation stages and were pooled for analysis. Embryos were monitored daily and fixed for analysis at different time points up to late germ band stages.

Results

The two stages that we sought to understand with this work are the “soccer ball stage” (S6 in Browne et al., 2005) and the “rosette stage” (S7 in Browne et al., 2005). We aimed to use lineage analysis to determine the extent of regularity in clonal patterns and cell–cell contacts at these two stages. The soccer ball stage is reached at ~12 h (at 25 °C) after egg-laying, and consists of approximately 100 cells. This stage is of interest because the cells are morphologically uniform and no fate map exists for all cells at this stage. The rosette stage consists of approximately 120 cells, and is reached at ~18 h (at 25 °C). This is just before gastrulation with the rosette-shaped arrangement of cells marking the site where gastrulation begins (Movie S1).

Extensive cell migration precedes gastrulation

An embryonic staging scheme and a fate map of the eight-cell stage blastomeres based on *in vivo* labeling techniques were previously established for *P. hawaiensis* (Browne et al., 2005; Gerberding et al., 2002). However, the existing staging descriptions do not describe how

the products of the eight-cell stage divide, move, and position themselves in order to begin gastrulation. In order to gain insight into the precise cleavage pattern, positional clonal distribution, and the migration behavior of the descendants of the eight-cell stage, we used 4D microscopy to trace the cell lineages of the third cleavage blastomeres. The principal wild type cell lineage analysis was composed from recordings of 17 different embryos that all developed normally compared to controls (non-recorded embryos), and hatched successfully. In some cases, fixed embryos, *in vivo* injections, and additional recordings were performed to confirm observed processes. Using the previously established nomenclature (Gerberding et al., 2002) for the third cleavage blastomeres in this species as a starting point, we have developed a nomenclature for the blastomeres from fourth cleavage onwards (Figs. 1A–C). This allowed us to assign specific lineage identities to all of the cells that make up the core of the gastrulation center (discussed below).

The first three cleavages in *P. hawaiensis* lead to the establishment of an eight-cell stage that is characteristic for amphipod crustaceans (discussed by Scholtz and Wolff, 2002). The first two cleavages give rise to a four-cell stage in which the ancestor blastomere to **Mav** and **g** (which we call "**Mav**/**g**") is identifiable as slightly smaller than the others. The third cleavage is perpendicular to the previous one and unequal, so that the eight-cell stage consists of the four macromeres **Mav**, **El**, **Er**, and **Ep**, and the four micromeres **g**, **ml**, **mr**, and **en** (Figs. 1A and 2A). In most embryos (73/87, 84%) the micromeres are positioned in a regular arrangement in which the opposing micromeres **ml** and **mr** share a contact plane, while **g** and **en** do not (Figs. 1A and D). 3% of embryos (3/87) have the opposite arrangement, with **g** and **en** sharing a contact plane instead of **ml** and **mr** (Fig. 1D). In 10% of embryos (9/87), no opposite micromeres share a contact plane, and instead contact only their left and right neighbors (Fig.1D). We performed lineage analysis only of embryos showing the majority arrangement of **ml**/**mr** contact planes (Fig. 1A). The observations presented hereafter thus refer only to embryos that showed this arrangement.

The third cleavage is the last synchronous cleavage. In the fourth cleavage the macromeres divide slightly ahead of the micromeres, with **g** being the last micromere to divide. The arrangement of the eight micromeres at the 16-cell stage can vary (Fig. 1E). Specifically, there is variation in the arrangement of the mesoderm micromeres (**mla**, **mlp**, **mra**, and **mrp**). In 75% of embryos (30/40), all mesoderm micromeres have contact with their left/right counterpart. In 16% of embryos (6/40), only one of the two left/right mesoderm micromere pairs are in contact with each other (Fig. 1E).

During subsequent cleavages synchrony is gradually lost, but within each clone, cleavage timing is fairly regular. In general, the macromeres undergo faster mitotic divisions than the micromeres. Therefore, when the size of the cells has become roughly homogeneous, the macromeres have gone through one or two more division cycles than the micromeres, and the embryos are designated as being at the soccer ball stage (S6 in Browne et al., 2005). The cell arrangement patterns before the rosette stage result from mitotic spindle orientation rather than active cell reorganizations, and will be

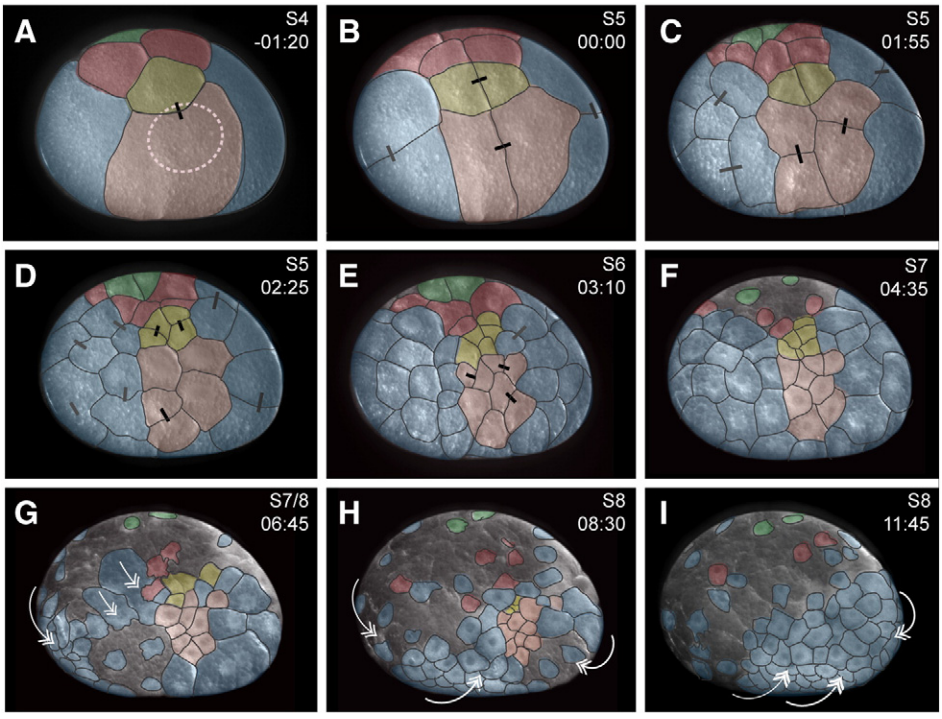

Fig. 2. Clonal domains and cell movements from eight-cell stage through gastrulation. The general processes of divisions and cell movements from the eight-cell stage through gastrulation are exemplified by still images of a time-lapse recording of one embryo (#01; see Table 1). The embryo is oriented facing the **g**/**Mav** side in all images. Stages indicated at top right of each panel are as per Browne et al. (2005); times shown are hh:min elapsed from 16-cell stage, which is set to 00:00 (B). Transparent colored overlay indicates clonal domains of third cleavage blastomeres as follows: **g** and progeny — yellow, **Mav** and progeny — orange, **ml**, **mr** and progeny — red, **en** and progeny — green, and **El**, **Er**, **Ep** and progeny — blue. Black bars in A–E indicate sister cell relationships of **g** and **Mav** and their progeny. (A) Eight-cell stage following third cleavage. White circle: region of the future formation of the rosette. (B) 16-cell stage following fourth cleavage. The first division occurs in the same direction in both **g** and **Mav**. (C) Cell arrangement of **g**/**Mav** descendants after fifth cleavage. The division plane of **Mav** descendants is perpendicular to that of the previous division. (D) Sixth cleavage. The fifth cleavage shown in (C) is the last near-synchronous cleavage cycle, and the number of cells therefore varies from this point onwards among embryos at the same stage. (E) The initial rosette, composed primarily of **g** and **Mav** descendants (yellow and orange cells respectively), is located around the former cell border that existed between **g** and **Mav** at the eight-cell stage (white circle in (A)). Those cells that will form the rosette move progressively closer together at this site. (F) Nuclei and their surrounding cytoplasmic masses begin to detach from the yolky cell bodies in the superficial progeny of **en**, **ml**, and **mr**. (G) **Er** descendants begin rapid movements (arrows) towards the rosette (gastrulation site) and will eventually regain contact with **Mav** descendants of the rosette. (H–I) The gastrulation site is the same region where the rosette formed earlier. The extensive cell rearrangements and cell migrations comprising gastrulation are largely driven by derivatives of **El**, **Er**, and **Ep** (arrows). **ml** and **mr** descendants also undergo extensive cell movements that are not indicated here. Ectoderm precursors derived from **El**, **Er**, and **Ep** expand towards the gastrulation site and initiate the closure of ectodermal sheets above the gastrulation site. **en** derivatives (green) remain in the same region throughout gastrulation (A–I).

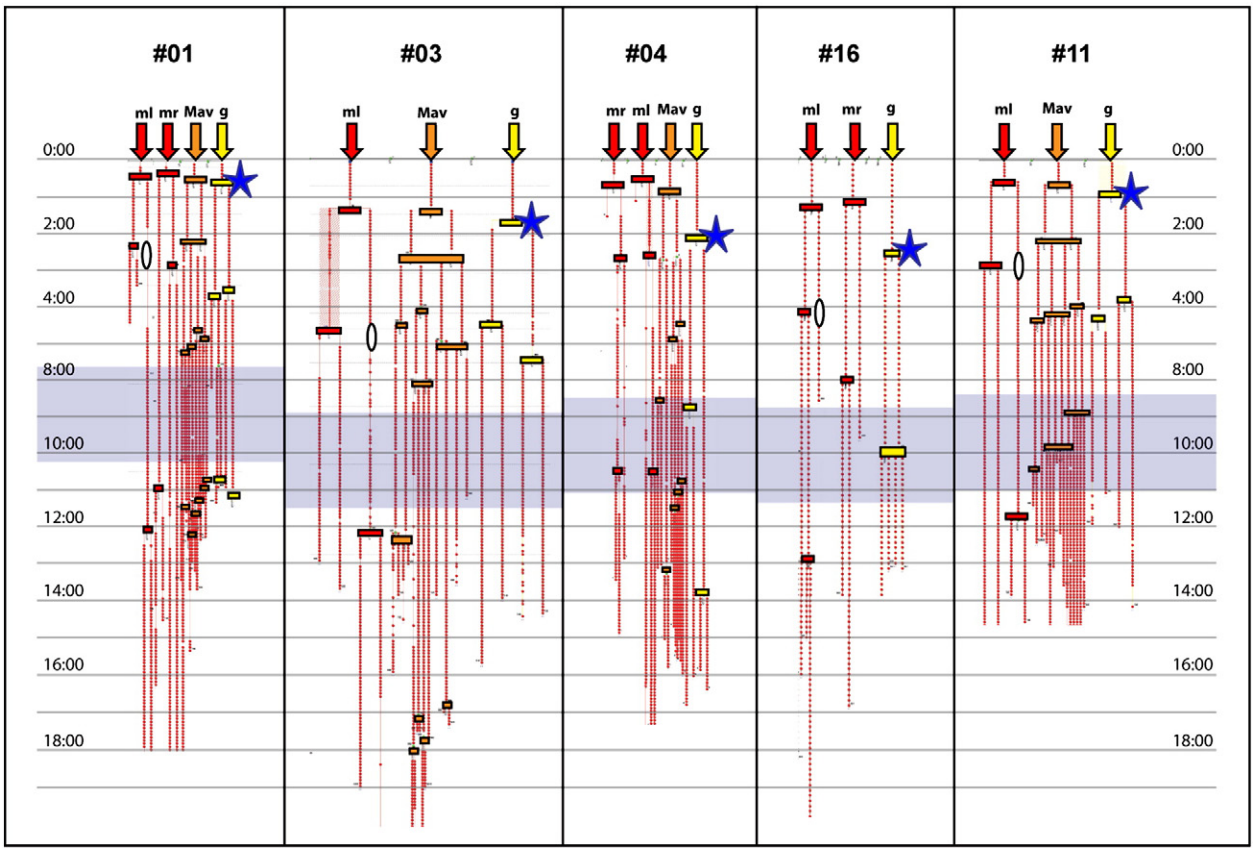

Fig. 3. Variation in timing of mesoderm and germ line cleavages between third cleavage and gastrulation. Lineage trees of five selected embryos (see Table 1) are shown for comparison (based on screen shots of SIMI°BioCell) showing the timing of division events for **g**, **ml**, **mr**, and **Mav** and their descendants. Arrows indicate the lineages of the germ line precursor **g** (yellow), the mesoderm precursors **Mav** (orange), and **ml** or **mr** (red). Rectangles of the corresponding colors indicate division events of each of these lineages. Blue shaded area represents the time at which embryos are at the rosette stage. Each of the lineages starts at the eight-cell stage (normalized here to 0:00 as the start point of the time lapse recordings) and covers the period up until gastrulation (at least 14 h starting from the eight-cell stage; times indicated by horizontal lines). Relative division timing follows a clear pattern: the first division of **g** (star) is delayed compared to the divisions of all other blastomeres. White ovals in the **m** lineages (embryos #01, #03, #11 and #16) indicate the divisions of **mla** and **mra** towards the interior of the egg; only the outer daughter cells (**mlao** and **mrao**) were traced through further development. Variability in absolute division times is likely due to the fact that recording start points may have been at different relative time points of the eight-cell stage.

described separately for each of the eight third cleavage lineages in the following sections.

Two cell groups of special significance for embryonic patterning emerge from the soccer ball stage. The first is the rosette, a small (approximately 12–16 cells) group composed of **g** and **Mav** progeny (Fig. 2E, yellow and orange cells). It is formed near the border of **g** and **Mav** lineages (Fig. 2A, white circle), and is the site of the first gastrulation movements *sensu stricto*. As observed previously the rosette stage starts around 12 h after fertilization, and lasts until 20 h (S7 in Browne et al., 2005). The second (approximately 48 cells) is a monolayered sheet of ectoderm precursors of the future germ band (Fig. 2E, blue cells), and is composed only of descendants of **El**, **Er**, and **Ep**.

During the divisions leading up to the rosette stage, a transformation in cell morphology is detected first in **en** clones, and then in the surrounding **El**, **Er**, and **Ep** progeny. The daughters of **en** do not move significantly from the original position of **en** (Fig. 2). They remain at the pole opposite the rosette until late gastrulation and germ band formation (discussed below). The first clear indications of cell migration then begin, approximately 12 h after egg-laying (~5 h after the eight-cell stage), when the first micromere derivatives move together to form the rosette (Fig. 2F).

At the eight-cell stage all blastomeres display uniformly distributed yolk, with the cytoplasm being concentrated around the nuclei. Nuclei are initially positioned relatively centrally within the cell, and then move gradually to a more apical position (towards the surface of the embryo). By 4-5 h after the eight-cell stage, the nuclei and their surrounding cytoplasm appear as small whitish patches with cytoplasmic threads extending through the cellular yolk mass, with the nuclei visible as darker spots (Movie S2). Within the next hour, these patches take on a slightly different appearance: under Nomarski optics they appear more transparent, with granules floating in the cytoplasm around the nuclei (Movie S2). The nuclei and surrounding cytoplasm then seemed to become detached from the remainder of the cell content (Figs. 2F–H), which remains as a yolky mass (Movie S1). The mechanism of this detachment is unclear in *P. hawaiensis*. However, in the amphipod *Orchestia cavimana*, the yolk is extruded from the blastoderm cells by a superficial cleavage in the absence of S phase (Scholtz and Wolff, 2002).

When these cells begin their directed migration, their morphology changes yet again: the cytoplasm begins to form protrusive structures which resemble filopodia (Movie S2), as has been described for many migrating cell types (Aman and Piotrowski, 2010). We observed this behavior in migrating cells of all somatic lineages. In these migrating cells, the nuclei move within the cytoplasm towards the direction of migration, so that the rest of the cytoplasm seems to follow the nucleus (Movie S2).

Derivatives of the germ line precursor **g** *show delayed divisions*

The first division of **g** creates left and right daughter cells **gl** and **gr** (Figs. 1B and 2B). This cleavage is delayed with respect to the divisions of the macromeres and the remaining micromeres. In 88% of embryos examined (15/17), the cleavage of **g** was delayed 10–60 min with

respect to other micromeres, and its cleavage was always delayed at least 5 min with respect to the division of **Mav** (Fig. 3).

The second division of **g** (i.e. the division of **gl** and **gr** into **gla**, **glm′**, **gra**, and **grm′** Fig. 1C) is also clearly delayed compared to the fifth division cycle of the remaining cells (Fig. 3). It usually occurs prior to the rosette stage, so that by rosette formation four germ line precursor cells have formed (Fig. 3). In 18% of embryos examined (3/17), the second division occurred much later in one or both of **gl** and **gr** (Fig. 3). Irrespective of the timing of divisions, the **g** derivatives remain clustered as a group throughout the rosette stage and gastrulation.

Derivatives of mesoderm progeny **mr** *and* **ml** *migrate both superficially and internally in the embryo*

ml and **mr** are the progenitors primarily of the left and right trunk mesoderm, respectively. Previous fate maps showed that some of their daughters give rise to the mesoteloblasts, which are mesodermal stem cells whose descendants populate each trunk segment (Gerberding et al., 2002). **ml** and **mr** divide only twice before the formation of the rosette, so that four derivatives of each cell are present at this stage.

The first division planes of **mr** and **ml** are perpendicular to the third cleavage plane. As a result, their anterior daughter cells (**mla** and **mra**) lie next to **gl** and **gr**, while their posterior daughters (**mlp** and **mrp**) lie next to **enl** and **enr,** respectively (Figs. 4A and B). The subsequent division planes of the posterior daughters **mlp** and **mrp** are again perpendicular to the previous plane, inclined towards the **en** derivatives (Fig. 4D).

The second division of **ml** and **mr** occurs about 2 h later, and before **g** undergoes its second division cycle (Fig. 3). Both anterior daughters of **ml** and **mr** (**mla** and **mra**) give rise to two cells with very different cellular behaviors and presumptive fates. Unlike previous mitoses, in which cleavage planes are parallel to the surface of the embryo, the cleavage planes of **mla** and **mra** are perpendicular to the surface of the embryo (Fig. 3, ovals in m lineages of embryos #01, #03, #11 and #16). This has the result that only one of the resulting daughter cells is clearly visible at the egg surface. These "outer" daughter cells, called **mlao** and **mrao**, remain at the egg surface until the rosette stage, when they come into direct contact with the descendants of **g** (Figs. 4E–H).

The second set of daughter cells of **mla** and **mra**, born underneath the egg surface, become "inner" cells (**mlai** and **mrai**) that ingress into the yolk and undertake independent lateral migration paths to the embryonic rudiment. Although these are the first cells to enter the embryo, we do not consider their movement the beginning of gastrulation. Instead, the later movements of **g** and **Mav** descendants at the rosette (gastrulation center) constitute the onset of gastrulation *per se* (described below).

mlai and **mrai** remain within the interior of the embryo until rosette formation, and then re-emerge on either side of the rosette close to the surface of the embryo (Fig. 4E). They are subsequently internalized and come to lie together with the posterior **ml** and **mr** descendants underneath the **El** and **Er** clones respectively. **mlai** and **mrai** are thus the likely progenitors of the mesoteloblasts.

Mav *gives rise to cells that contribute to the rosette*

Mav undergoes divisions to produce up to eight cells before rosette formation (Figs. 2E and 3). The first division plane is parallel to that of micromere **g** (Fig. 2B). The first two divisions of **Mav** generally occur simultaneously with those of the ectodermal founder cells **El** and **Er**.

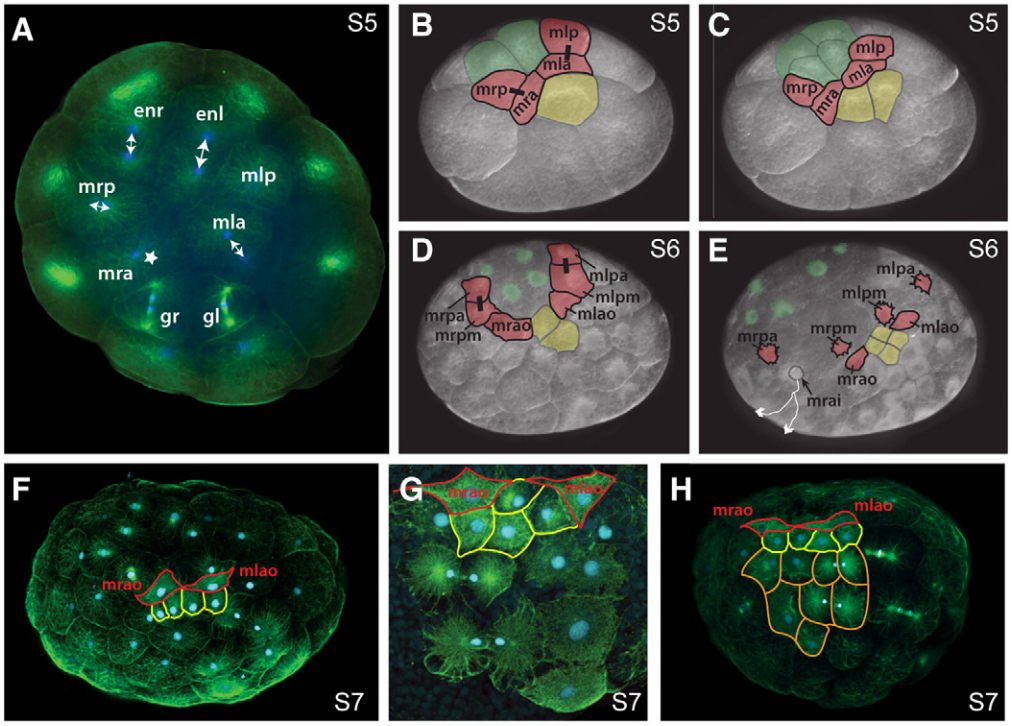

Fig. 4. The behavior of **ml** and **mr** derivatives before the rosette stage. (A) Confocal micrograph of the micromere pole of a 16-cell embryo. The spindle orientation of cleaving somatic micromeres is shown (double-headed arrows). The delayed division of **gl** and **gr** that is observed with 4D microscopy is greater at the level of cytokinesis than at the level of spindle formation. mra (IN BOLD) spindle formation has not yet begun (star). (B–E) Cleavages and movements of the **mra** and **mla** lineages over time. (B) The cleavage of **mra** and **mla** occurs before cleavage of the **g** and **en** derivatives. (D) Only one of the two daughter cells of **mra** and **mla** is visible on the surface of the yolk (outer daughter: **o**), while the second daughter cell sinks into the yolk mass and is not superficial (inner daughter: **i**). (E) In some recordings, the inner cells **mrai** and **mlai** are visible below the surface (black arrow), and can be seen to migrate laterally (white arrows). (F) The outer cells **mrao** and **mlao** (red) form part of the gastrulation center and are in direct contact with **g** descendants (yellow). (G) Higher magnification of the forming rosette. The arrangement of **g** descendants relative to **mrao** and **mlao** (red) is not invariant, but the direct contact between **mrao**/**mral** and at least two **g** derivatives is preserved in all embryos. (H) Near-rosette stage embryo rotated slightly towards the anterior, showing the **Mav** cells (orange) at the posterior of the rosette, four of which are in direct contact with the **g** descendants (yellow). Green = alpha tubulin; blue = nuclei (DAPI). Stages indicated in each panel are as per Browne et al. (2005).

During subsequent division cycles, further **Mav** progeny may be delayed in division frequency relative to the ectodermal cells (Figs. 2D and E). However, these delays do not show regular patterns within specific **Mav** sublineages, and become increasingly asynchronous over time (Fig. 3). Similarly, following the second cleavage (which occurs 1 to 2 h after the first), the division timing of **Mav** progeny cells is increasingly variable (Fig. 3). Despite this variability, by the time of the rosette stage, there are always eight to ten cells of **Mav** progeny at the center of the rosette (Fig. 2E). Up to four of these (usually **Mavrar**, **Mavral**, **Mavlal** and **Mavlar**) are in contact with **g** descendants at this stage (Figs. 2E and 4H).

Ep *progeny provide a landmark for clonal identification of all cells at the "soccer ball" stage*

El, Er, and **Ep** divide synchronously for four divisions, and subsequently their cleavages become asynchronous (Figs. 5 and 6). Before rosette formation, the ectoderm precursors can undergo up to five to six divisions and therefore exhibit the highest proliferation rate of all blastomeres at this stage (Fig. 6). The first division planes of **El** and **Er** are perpendicular to the previous cleavage planes (Fig. 2B). The subsequent division planes of **Ela**, **Elp**, **Era**, and **Erp** are again oriented perpendicular to the previous planes, and are parallel on each side of the embryo (Fig. 2C).

The division pattern of **Ep** is regular and bilaterally symmetrical for three cleavage cycles beginning with the 16-cell stage (Figs. 5A–E). This cleavage pattern bilateral symmetry is much more striking than that observed in the cleavages of the blastomere pairs **El**/**Er** or **mr**/**ml**, which are the other two bilaterally symmetrical germ layer founder cell pairs in the embryo. The first cleavage plane of **Ep** (fourth cleavage) is parallel to those of the micromeres **en** and **g** (Fig. 5B). The cleavage planes of the daughter cells **Epl** and **Epr** (fifth cleavage) are perpendicular to the previous cleavage. This division gives rise to two smaller cells (**Epla** and **Epra**) that are adjacent to **en** progeny, and two larger cells (**EplM′** and **EprM′**) (Fig. 5C). The subsequent cleavage plane (sixth cleavage) is again perpendicular to the previous one, so that the daughter cells are arranged in two rows of four cells each (Fig. 5D). The row towards the **en** derivatives comprises the smaller cells **Eplal**, **Eplar**, **Epral**, and **Eprar**. The second row, towards the derivarives of **El** and **Er**, is made up of the larger cells **EplM′l**, **EplM′r**, **EprM′l**, and **EprM′r** (Fig. 5D).

After the four cells towards the **en** progeny (**Eplal**, **Eplar**, **Epral**, and **Eprar**) undergo another round of division which is again perpendicular to the previous division (Fig. 5E), they cease dividing and undergo the morphological transformation described above, whereby the nucleus and cytoplasm are visible at the surface of the embryo and become migratory (Figs. 5F–H). In contrast, the other four cells (**EplM′l**, **EplM′r**, **EprM′l**, and **EprM′r**), which lie closer to the future ectodermal germ disk (mainly the progeny of **El** and **Er**), undergo even more than one division and begin movement towards the region of the rosette on the other side of the embryo (Figs. 5G and H, arrows).

The invariant clonal arrangement and morphologies of **Ep** and **en** that we identify here may now provide landmarks for the *in vivo* identification of the clonal origin of cells at the soccer ball stage without the need for previous cell labeling.

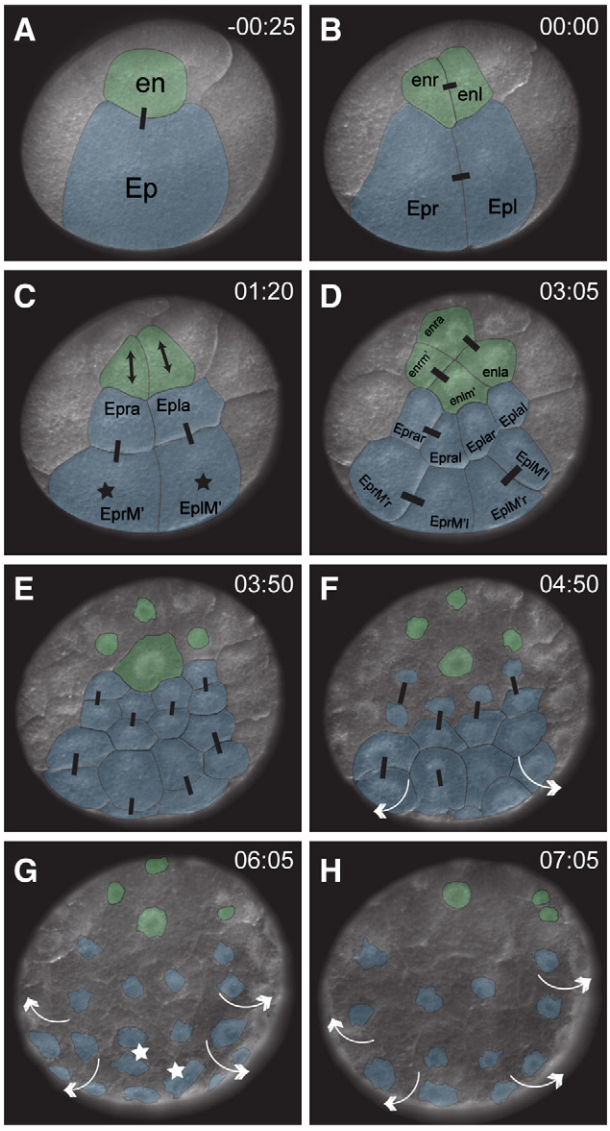

Fig. 5. The cleavage pattern and cell movements of **en** and **Ep** from the eight-cell stage to the rosette stage. Still frames from the time-lapse recording of a single embryo (#15); see Table 1) are shown in all panels. The embryo is oriented with view of **en**/**Ep** in all images, (transparent overlay: **en** and progeny — green, **Ep** and progeny — blue). Black bars indicate sister cell relationships. Stages indicated at top right of each panel are as per Browne et al. (2005); times shown are hh:min elapsed from fourth cleavage (B), which is set to 00:00. (A) Eight-cell stage. (B) The first division of both **en** and **Ep** runs meridionally. (C) The second division runs equatorially in both clones (double-headed arrows indicate spindle orientation in **en**). In **Ep** the second division results in two smaller cells neighboring the **en** progeny and two larger cells (indicated by asterisks, size not fully visible here due to orientation). (D) The third division cycle plane is perpendicular to the previous one. (E) The fourth division is again perpendicular to the previous one and is the final regular, synchronous division of the **Ep** clone. Here three descendants of **en** have condensed their cytoplasm around the nucleus (visible margin of cytoplasm outlined in black) and have shed the yolky cell body. (F) The **Ep** progeny adjacent to **en** progeny start to shed their yolky cell bodies and begin a lateral movement towards the progeny of **El** and **Er** (arrows). (G–H) The movement of the **Ep** progeny towards the condensation of all ectoderm precursors proceeds (arrows); only a few **Ep** descendants divide during this migration period (stars in G). **en** progeny remain in the same region as the original position of **en** up until germ disk formation.

The clonal composition of the rosette is stereotyped

Previous fate maps had indicated that the cells at the center of the rosette were of mesodermal and germ line origin, flanked by ectodermal cells (Gerberding et al., 2002; Price, 2005; Price and Patel, 2008). Our lineage analysis confirms this composition (Fig. 6), and further, shows that the cells of the rosette have specific lineage identities (discussed below). The four germ line progenitors (**gra**, **grm**, **gla** and **glm**, yellow cells in Fig. 6) lie adjacent to each other and are flanked on the anterior side by **mrao** and **mlao** (red cells in Fig. 6). On the posterior side, the germ line progenitors are in contact with the eight descendants of **Mav** (pink cells in Fig. 6), generally with the anterior descendants of **Mav**. Further away from the core of the rosette, the posterior descendants of the mesoderm micromeres and all four endodermal descendants (**enla**, **enlm′**, **enra** and **enrm′**) retain

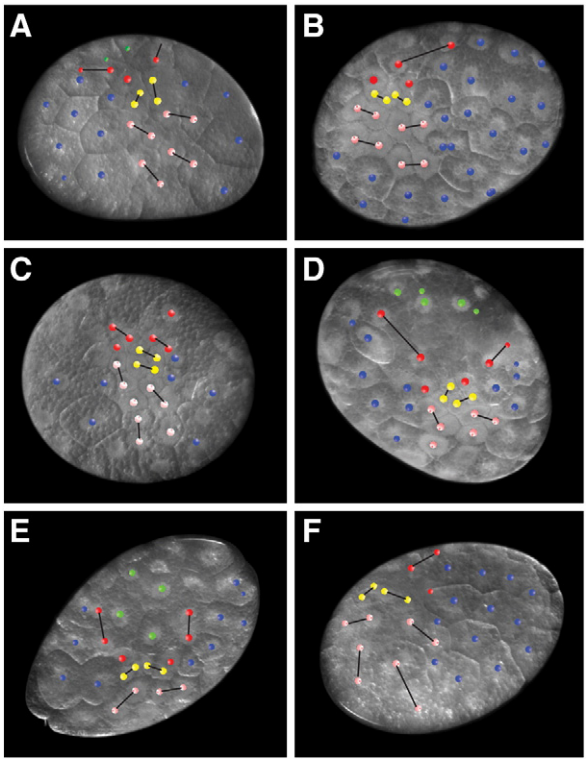

Fig. 6. The clonal composition of the rosette stage is invariant. All panels show rosette stages (S6/S7 of Browne et al. (2005)) of different embryos whose complete lineages up until gastrulation were traced using SIMI°BioCell. Live white incident light views of embryos are superimposed with 3D models generated by SIMI°BioCell indicating position of nuclei. Colored circles indicate nuclei of descendants of **g** (yellow), **Mav** (pink), **ml**/**mr** (red), **en** (green) and ectoderm precursors **El** or **Er** (blue). Black lines indicate sister cell relationships, showing that while the clonal distribution in the rosette stage is regular, the divisions of the clones show no regular pattern.

their amoeboid morphology on the surface of the yolk (Movie S2, Fig. 4, green cells in Fig. 6). In contrast, the ectoderm descendants are in the process of forming a continuous epithelium at the posterior and lateral sides of the rosette, in direct contact with **Mav's** descendants.

While this clonal distribution at the rosette stage is consistent, the spindle orientations of cleavages leading up to this arrangement show no regular pattern (black lines in Fig. 6). This suggests that the specific cell–cell contacts found in the rosette are the result of active cell movement, rather than oriented cell divisions.

Gastrulation proceeds by both immigration and epibolic movements

The first cells to undertake gastrulation movements *per se* are the four **g** progeny (**gla**, **glm′**, **gra**, and **grm′**), which immigrate below the somatic rosette cells by detaching from the monolayer of the rosette arrangement (Fig. 2H, Movie S2). They immigrate either as single cells (in random order) or as a group of cells, and come to lie underneath the surrounding cells, which are descendants of **Mav**, **El** and **Er** (Movie S2). The *P. hawaiensis* gastrulation center thus forms as a result of multiple cellular ingressions without forming a clearly visible blastopore, rather than collective cellular invagination movements. This is in contrast to reports on gastrulation in the amphipod *Orchestia cavimana*, where the blastopore is formed by invagination and is clearly visible as an indentation (Scholtz and Wolff, 2002). Immediately following the movement of the four **g** progeny, the outer descendants of **ml** and **mr** (**mrao**, **mrpm**, **mrpa**, **mlao**, **mlpm**, and **mlpa**) immigrate below the ectoderm on the lateral sides of the rosette (Figs. 2G–I). Accompanying this immigration, ectodermal cells shift via epibolic movements, coming to lie above the germ line and **Mav** derivatives (Fig. 2G, white arrows). The remaining gastrulation movements comprise extensive cell rearrangements and cell migrations by derivatives of **El**, **Er**, and **Ep** (Figs. 2G–I, arrows, Figs. 5F–H).

Regulative changes in cell behavior do not occur before gastrulation

P. hawaiensis embryos are known to be capable of regulative replacement of mesoderm and ectoderm, if precursors of these germ layers are ablated before the germ band stage (Price et al., 2010). Having characterized the normal cleavage and migration behaviors of each of the third cleavage blastomeres, we wished to investigate whether regulative changes in cell fate determination began in early cleavage stages. To begin to address this, we analyzed the lineage patterns and cell behaviors of embryos whose **mr**, **ml**, **g** or **en** blastomeres had been ablated at the eight-cell stage (Fig. 7).

Immediately following ablation, the timing and orientations of mitosis were slightly irregular in the remaining micromeres. These differences from control embryos are likely due to the physical absence of the ablated micromere, as the remaining micromeres sometimes “spread out” slightly into the space vacated by the ablated cell (Fig. 7, compare A with B–D). After the first two or three cleavages, however, overall cells continued to cleave, change morphology and migrate as did the cells of control embryos (Fig. 7). Cell trajectories towards the rosette were essentially unchanged, and the rosette itself formed with the same spatial and clonal composition as control embryos, with the exception of the missing lineage cells (Fig. 7, compare A3 with B3-D3). Together with previous observations (Price et al., 2010), this indicates that the regulative changes in cell behavior and fate that allow the replacement of ablated lineages are likely to take place in the short (~32 h) window between gastrulation and early germ band formation. However, we cannot rule out the possibility that new cell-cell contacts formed when micromeres are ablated may play a role in the regulative replacement of lost lineages.

The relatively unchanged behavior of the remaining cells following micromere ablation also raises the possibility that the cellular behaviors up to and including rosette formation and gastrulation are largely the result of maternally inherited instructions, rather than zygotically transcribed gene functions. To test this hypothesis, we blocked transcription in embryos by subjecting them to continuous incubation in alpha-amanitin, which is an inhibitor of RNA Polymerase II (Jacob et al., 1970), and then observed the overall morphological effect on early development (Fig. 8). Embryos in which transcription was pharmacologically inhibited proceeded through development normally until the onset of gastrulation (Table 2, Figs. 8A and B). At the beginning of gastrulation, immigration of **g** and **Mav** precursors continued as in control embryos. However, subsequent cell movements became abnormal: cells of the inner layers (mesoderm and germ line) continued their immigration and sank into the yolk mass, creating an irregular pit (Fig. 8 compare A1 and A2 with B1 and B2). Due to this condensation of nearly all cells, the rest of the embryo consists only of a yolk mass (Fig. 8B2). The epibolic movements and epithelial integrity of the overlying ectodermal cells were lost. Instead, these cells took on a rounded, detached morphology and began to detach from the germ rudiment, reminiscent of an epithelial to mesenchymal transition (Fig. 8 compare A3 with B3).

Discussion

The cell lineages determined in this study, and the median timing for each mitosis, are summarized in Fig. 9 (Fig. S1 shows the extent of cleavage timing variability for each lineage).

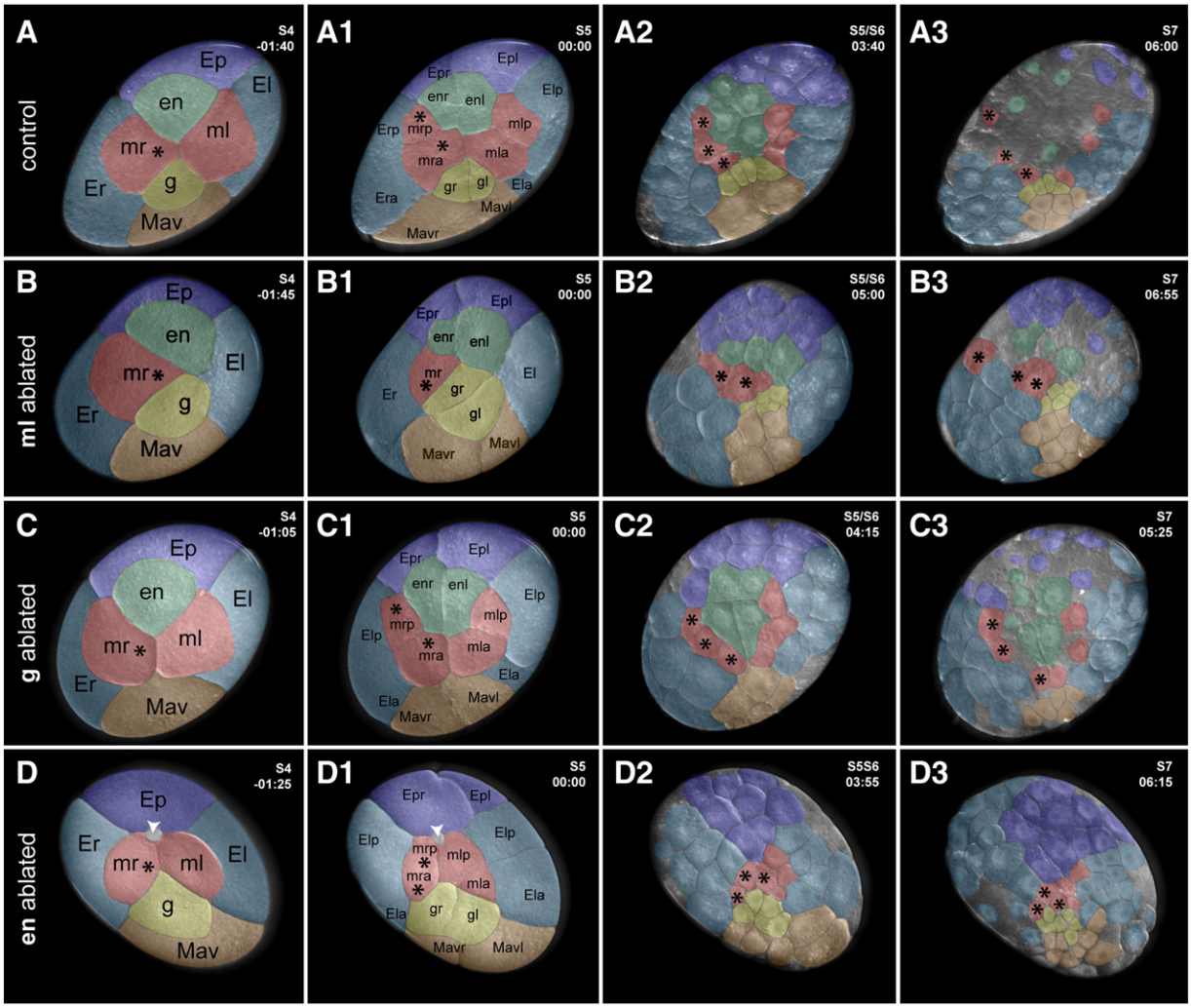

Fig. 7. Patterns of cleavage and migration before gastrulation are unaffected by loss of micromeres. Wild type embryos (A–A3) compared with embryos in which **ml** (B–B3), **g** (C–C3) or **en** (D–D3) was ablated at the eight-cell stage. **ml** descendants (black asterisks) are indicated for orientation, to show that the relative arrangements of clones are unaltered in micromere-ablated embryos compared to controls. All embryos are oriented with **Mav** down. Transparent colored overlay indicates clonal domains of third cleavage blastomeres as follows: **g** and progeny — yellow, **Mav** and progeny — orange, **ml**, **mr** and progeny — red, **en** and progeny — green, **El**, **Er** and progeny — blue, and **Ep** and progeny — purple. Embryos are compared at the eight-cell stage (column A–D), between third and fourth cleavage (column A1–D1), close to rosette stage (A2–D2) and just following the rosette stage (A3–D3). Arrowheads in (D, D1) indicate tiny remnant of **en** cytoplasm which has disappeared by the rosette stage (D2). Images in each row are still images from time-lapse recordings of the same embryo. Stages indicated at top right of each panel are as per Browne et al. (2005). Times shown are hh:min elapsed from the 16-cell stage, which is set to 00:00 (column A1–D1).

Predictable clonal patterns at a morphologically homogeneous stage

Among embryos from the same brood, which are fertilized near-simultaneously (Borowsky, 1990), early cleavages are initially clearly synchronous. However, the regular and synchronous timing of these cleavages decreases gradually over time. Our analysis shows that despite this apparent variability at a macroscopic scale, several invariable characteristics are identifiable between clones and between embryos of the same absolute age (h after first cleavage) at a cell lineage scale: (1) After fourth cleavage, synchrony decreases between lineages quite rapidly, but remains higher within a given lineage. (2) The macromeres divide more rapidly, but at less predictable absolute times, than the micromeres. (3) The transition to migratory cell morphologies, directions and migration behaviors of cells is predictable within a given clone. (4) As a result of (2) and (3), a reproducible mosaic pattern of cells of all germ layers and the germ line can be identified at the "soccer ball stage." Previous studies had noted that the uniform appearance of all cells at this stage, and the difficulty of identifying embryonic polarity by using overall egg shape, made it difficult to reproducibly assign precise lineage identities to each cell or polarity to the forming embryo (Gerberding et al., 2002). The most critical stages for understanding the earliest manifestations of cell fates following germ layer establishment at the eight-cell stage, are those in the period between the eight-cell stage and the completed germ disk (S4 to S8 from Browne et al., 2005). By adding cellular-level resolution to these stages (S5–S7), we have provided landmarks that allow clonal composition, and even certain specific cellular identities, to be determined at the soccer ball stage. Either the unique morphology of **g** descendants (often smaller than other cells, Figs. 2C–E) or the invariant cell number and spatial arrangement of the **en** and **Ep** clones at this stage (Figs. 5C and D) can provide landmarks to orient the embryo and determine the clonal identities of other cells at this stage, without the need for injection of lineage tracers (Gerberding et al., 2002) or newly performing 4D microscopy (this study). Identifying cells in this way should prove useful for future studies, including, for example, in situ hybridization screens to identify uniquely distributed transcripts associated with specific germ layers before gastrulation.

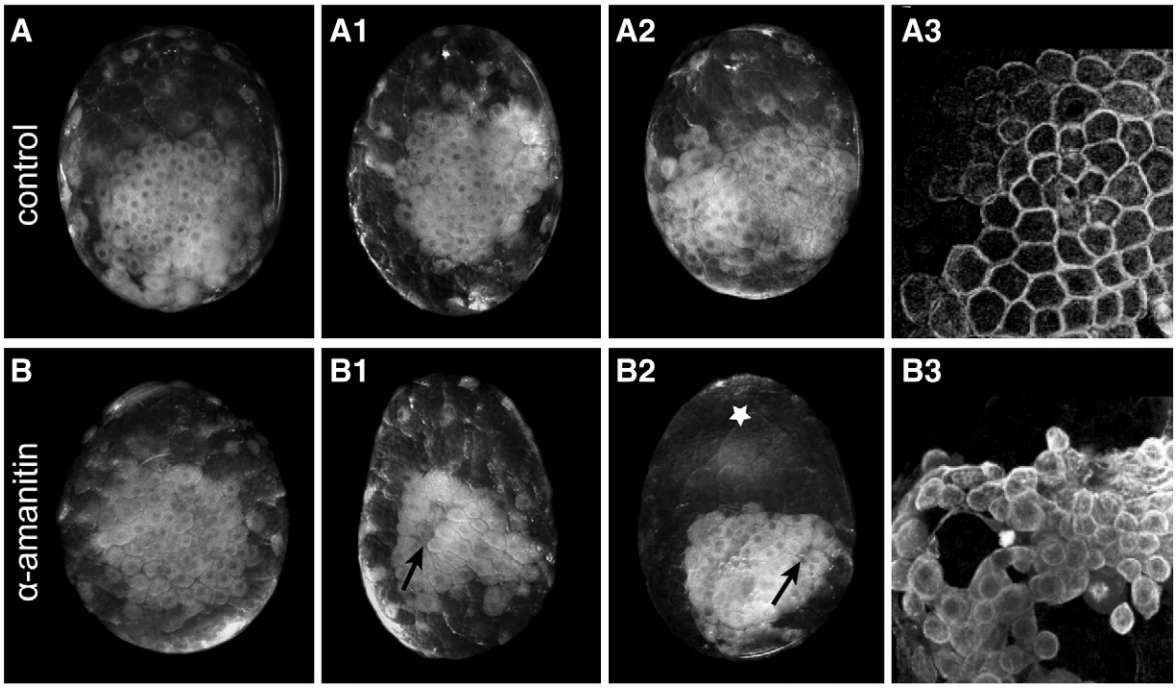

Fig. 8. Cell divisions, migrations and gastrulation in the absence of zygotic transcription. Wild type embryos (A–A3) and embryos in treated continuously with alpha-amanitin (B–B3). Treated embryos form normal embryonic rudiments 24 h after fertilization (compare A with B) but cannot form germ bands over the subsequent 24 h (compare A1 with B1). (B1) In the region of the inward movement of the cells a large blastopore-like indent is formed (arrow). (B2) The epithelial integrity of the germ rudiment is lost around the time of gastrulation (compare A2 with B2). All cells are condensed only in the region of the inwards movement (arrow) so that the rest of the embryo consists of mostly yolk mass (asterisk). (A3) and (B3) are projections of confocal sections of control and treated embryos of the ectoderm sheet of the germ disk at S8/9, respectively, labeled with anti-α tubulin. The regular ectodermal monolayer found in wild type embryos (A3) is disrupted in α-amanitin treated embryos in which the ectodermal cells take on a round shape and lose their epithelial integrity (B3).

Gastrulation in amphipods

The first three cleavages and the arrangement of the blastomeres during the four-cell and the eight-cell stages are typical characters for amphipod crustaceans, and are suggested to be apomorphic characters for the amphipods (Scholtz and Wolff, 2002). Moreover, several processes between these cleavages and the onset of gastrulation, described here for *P. hawaiensis*, reveal many similarities to what was found in the gammarid amphipod *O. cavimana* (Scholtz and Wolff, 2002; Wolff and Scholtz, 2002). In *O. cavimana* macromeres divide faster than the micromeres from the 16-cell stage onwards. However, the cleavage pattern described for the macromeres of *O. cavimana* up to the 128-cell stage is more invariant than that observed for *P. hawaiensis*. Macromeres **B**, **C** and **D** in *O. cavimana*, which correspond to **Er**, **Ep** and **El** in *P. hawaiensis*, undergo an unequal fifth cleavage. The largest daughter cell of each lineage then proceeds to divide with cleavage planes oriented in parallel to those of previous divisions; this is described as a "stem cell like" division mode. In contrast, in *P. hawaiensis* a stereotyped division pattern among ectodermal blastomeres was observed only in the division of **Ep** (Fig. 5). However, the cleavage planes of **Ep** and its descendants are perpendicular to that of the previous division (Figs. 5B–D) until the migration processes that immediately precede gastrulation begin (Figs. 5E and F).

In *O. cavimana* the onset of gastrulation becomes visible as a sickle shaped cell aggregation of approximately 20 cells that is formed around the germ line cells (corresponding to **g** descendants in *P. hawaiensis*) and mesendoderm cells (corresponding to **Mav** descendants)(Wolff and Scholtz, 2002). Gastrulation proceeds by an epibolic movement of derivatives of the left and right ectoderm precursor cells (corresponding to **El** and **Er**) combined with the simultaneous immigration and invagination of the mesendoderm cells and the germ cells. This results in the formation of a clearly visible blastopore in the anterior region of the germ disk (Scholtz and Wolff, 2002). In *P. hawaiensis* a sickle-like shaped cell arrangement is not formed, and a blastopore (as a clear indentation in the cell layer) does not appear during gastrulation. However, the rosette in *P. hawaiensis* and the sickle-shape formation in *O. cavimana* form at the comparable stages of gastrulation initiation, and the clonal arrangement of cells during the beginning of gastrulation is similar. In both amphipods the derivatives of the third cleavage germ line progenitor and its sister cell form the center of the initial gastrulation movements. These cells are then overgrown by the macromere derivatives that give rise to the left and right ectoderm.

Comparison with cell lineage of other malacostracan crustaceans

Cell lineage analyses on other malacostracans have largely been confined to two other holoblastically cleaving groups, euphausiaceans and dendrobranchiate shrimp. Although these two groups differ in the lineage of mitotically delayed cells called crown cells (Alwes and Scholtz, 2004), they display a striking number of early embryonic similarities that strongly suggest homologies at the cell lineage levels. These include invariant cleavage patterns for up to four synchronous cleavage cycles, mirror-image patterns of cleavage, radial division of crown cells, and the establishment at the 32-cell stage of two enlarged mesendoderm cells that become cleavage-delayed and give rise to endoderm or mesoderm and germ line (Taube, 1909). *P. hawaiensis*

Table 2
Effect of blocking transcription on early embryogenesis. Experimental embryos were treated with α-amanitin, and control embryos were exposed to equivalent final concentrations of DMSO as described in Methods.

	n	% survival		
		To soccer ball stage	To germ rudiment stage	Past germ band stage
Control	10	100	100	90
α-amanitin	74	100	100	0

cleavage does not possess any of these characteristics, and invariant cleavage and spatial patterns persist for a relatively short embryonic time period. The relatively higher flexibility of cleavage times and spatial arrangements in *P. hawaiensis*, which also increases over time until and including gastrulation, may be related to the high degree of embryonic somatic regulation displayed by this embryo (Price et al., 2010). The extent of regulatory potential in euphausiacean or dendrobranchiate shrimp embryos has not been tested. However, blastomere isolation studies on mesoderm in the shrimp *Sicyonia ingentis* have shown that cell fates and cleavage behaviors, including the ability of the two mesendoderm cells to influence the cleavage planes of adjacent blastomeres, are autonomous (Hertzler et al., 1994). This suggests that somatic cell fates and potentials in this embryo may indeed be autonomously determined to a greater degree than in *P. hawaiensis*. Future studies on isolated somatic blastomeres of *P. hawaiensis* will be necessary to confirm whether the regulatory properties observed in whole embryos (Price et al., 2010) are non-autonomous and reliant on zygotic transcription, as our study suggests.

Delayed division of the germ line

One aspect of *P. hawaiensis* cleavage that is consistent with embryogenesis in several other invertebrates, is the delayed and limited division of the germ line precursor **g** with respect to the somatic blastomeres. Within crustaceans, this delay is observed not only in amphipods (Langenbeck, 1898; Scholtz and Wolff, 2002) and other malacostracans (Biffis et al., 2009; Hertzler and Clark, 1992; Pawlak et al., 2010), but also in branchiopods (Kühn, 1908; Kühn, 1911) and copepods (Amma, 1911; Fuchs, 1914). Similarly, in hexapods with early-specified germ lines (see for example Klag and Swiatek, 1999; Poulson, 1947) and in several nematode worms (Skiba and Schierenberg, 1992), once the germ lineage is established, mitotic divisions slow with respect to somatic cells. A notable similarity among all of these organisms is that the germ line is known or strongly suspected to be determined by the inheritance of maternally supplied cytoplasmic determinants (see for example Amma, 1911; Extavour, 2005). This suggests that among the germ line characteristics conferred by "germ plasm" may be a specific and delayed cleavage pattern, which is preserved until much later in development, when mitosis resumes at gametogenesis.

Cellular behaviors during gastrulation

Our observations of gastrulation in *P. hawaiensis* are essentially consistent with the descriptions of this process as "multistage" in previous fate map analyses (Price, 2005; Scholtz and Wolff, 2002). However, in contrast to a previous analysis on *P. hawaiensis* (Price, 2005), but consistent with observations on the closely related amphipods *Microdeutopus gryllotalpa* (Langenbeck, 1898) and *Orchestia cavimana* (Scholtz and Wolff, 2002), we observed that **g** descendants were the first to immigrate at the gastrulation site, and not **Mav** descendants. However, as discussed further below, this immigration is not required for the completion of gastrulation or embryogenesis (Extavour, 2005; Price et al., 2010).

We have also found that the very first cells to move beneath the surface of the embryo do so prior to gastrulation *per se*, and are descendants of neither **g** nor **Mav**. We show these to be **mlai** and **mrai**, two second generation descendants of **mr** and **ml**, which delaminate towards the egg interior prior to the true gastrulation movements.

Our 4D analysis has revealed that the invariant positions of the cells at the rosette stage are not achieved by oriented cell divisions but rather by cell rearrangements. This is in contrast to what has been observed in other malacostracan embryos (see Discussion and references above). For example, in the shrimp *Sicyonia ingentis*, the two mesendoderm cells orient both the cleavage planes and the invagination directions of adjacent cells, and gastrulation cannot proceed without them (Hertzler and Clark, 1992; Wang et al., 2008). This property of the mesendoderm cells is autonomous (Hertzler

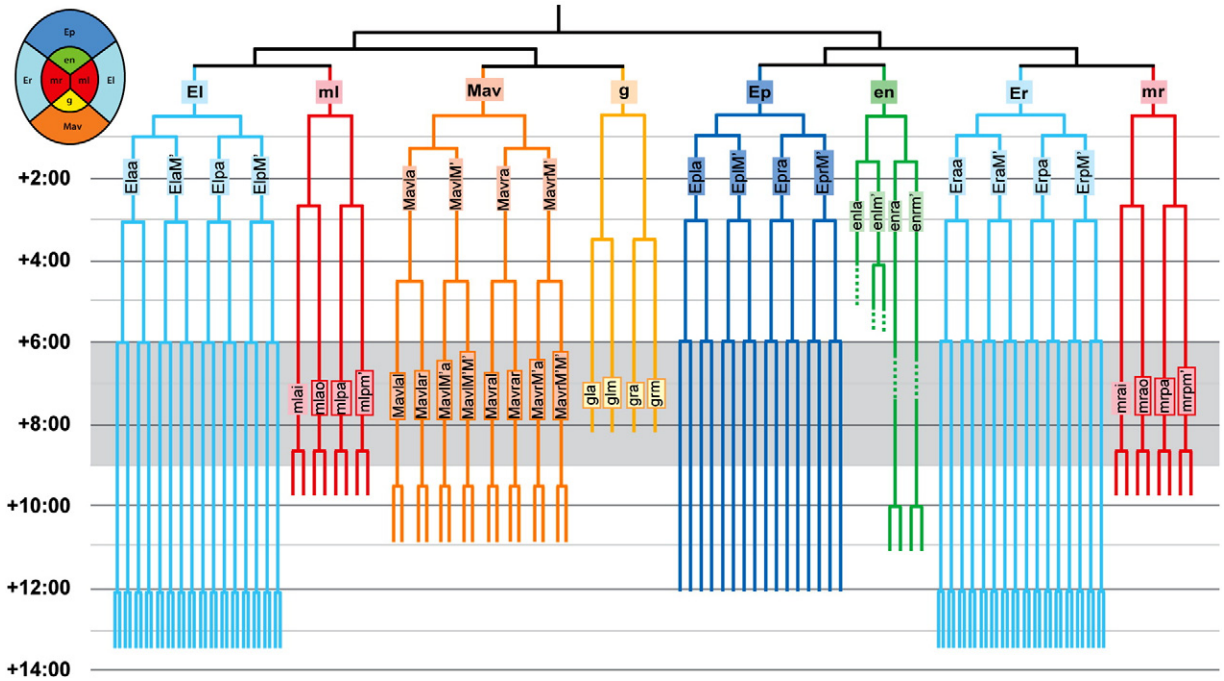

Fig. 9. Summary lineage of *P. hawaiensis* from the eight-cell stage up until the rosette stage. The information from all analyzed wild type embryos is summarized here. Cleavage times shown are median cleavage times (see Supplementary Fig. S1 for lineage-specific cleavage time ranges). Cell names according to the nomenclature outlined in Fig. 1C are shown for fifth cleavage derivatives. Cell names in boxes outlined with dark colors indicate the primary cells of the rosette stage (see Fig. 10). Gray shading in the background indicates the time at which embryos reach the rosette stage.

et al., 1994). However, in such dendrobranchiate shrimp, as well as in euphausiaceans, gastrulation begins at a stage with fewer cells than in *P. hawaiensis*. For example, in *S. ingentis* gastrulation begins at 6th cleavage, when there are only 62 cells. The primary role of cell rearrangements in *P. hawaiensis* gastrulation is therefore more similar to other animal embryos in which gastrulation involves large numbers of cells (Stern, 2004). This contrasts with animals gastrulating with few cells such as *C. elegans* (Lee and Goldstein, 2003), ascidians (Conklin, 1905) or decapod shrimp, where oriented cell divisions, whether intrinsically or extrinsically determined, may be critical.

Specific cell-cell contacts at gastrulation

While it was previously known that reproducible neighbor arrangements of specific germ layer clones contributed to the rosette (gastrulation center), we have now determined the specific cellular identities of cells at this stage (Fig. 10). Moreover, certain cellular contacts between the cells of the rosette are present in every wild type embryo at this stage. **mlao** and **mrao** each always contact at least one of the germ line precursors from the corresponding left or right side (Fig. 10, upper thick black lines). The posterior border of the germ line clone usually contacts no more than four of **Mav**'s eight descendants at this stage, and likely always the anterior descendants of **Mav** (one or more of **Mavrar**, **Mavral**, **Mavlal** or **Mavlar**; Fig. 10, lower thick black lines). Finally, the posterior and lateral borders of the **Mav** clone are always in contact with **Ep** and **El**/**Er** descendants, respectively (Fig. 10, white lines). Both gastrulation movements and the requirement for zygotic transcription begin shortly after this stage. The consistent arrangement of cells at this stage suggests that the molecular mechanisms driving gastrulation movements in wild type embryos may involve signaling processes at these conserved clonal/cellular interfaces. However, gastrulation can occur normally in the absence of any or all of the third cleavage mesoderm precursors (**Mav**, **ml** or **mr**), or any one of the ectoderm precursors (**Ep**, **El** or **Er**) (Price et al., 2010). Our transcriptional inhibition experiments showed that while immigration movements of **g** and **Mav** descendants are initiated normally, the epibolic movements of **Ep**, **El** and **Er** descendants cannot proceed in the absence of zygotic transcription (Fig. 8). We also observed that in the absence of a given micromere, the remaining clones did not alter their relative positions or behaviors, but rather simply came to "fill the space" created by the missing clone, thus creating novel neighbor relationships (Fig. 7).

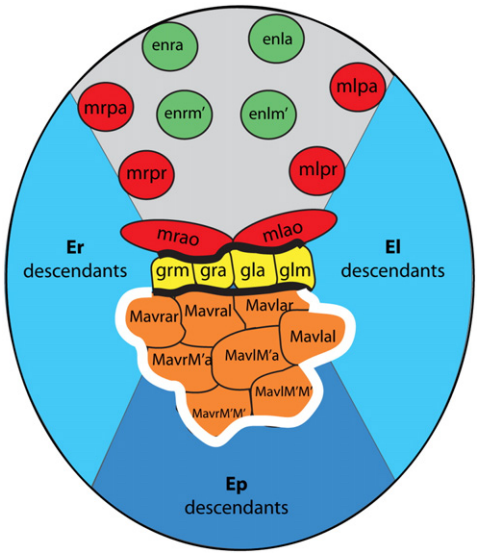

Fig. 10. Scheme of lineage identities and cell contacts of the primary cells of the rosette. Schematic representation of the late rosette stage showing lineage identities of cells that make up the future gastrulation center. For **en** derivatives, lineage identities of these cells were inferred with the assumption that their positions relative to each other do not change during their minimal migration up to the rosette stage (Fig. 5). The arrangement of specific **g** and **Mav** derivatives represented here shows variation in different embryos, for example the arrangement of **g** derivatives can be linear or more packed (compare to Figs. 4A and G). Invariant cell contacts are indicated by thick black lines (proposed to be dispensable for autonomous ingression gastrulation movements – see Discussion) or thick white lines (proposed to be necessary for non-autonomous epibolic gastrulation movements – see Discussion). **g** derivatives — yellow; **Mav** derivatives — orange, **ml** and **mr** derivatives — red, **en** derivatives — green.

Taken together, these data lead us to speculate the following model regarding the roles of autonomous and regulative control mechanisms of gastrulation in *P. hawaiensis*: in wild type embryos, the initial ingression of **Mav**, **ml**, **mr** and **g** descendants at the gastrulation center is directed by maternally provided factors and does not require non-autonomous signals with neighboring cells. Thus, gastrulation can proceed normally in the absence either of zygotic transcription or of any given mesoderm precursor. In contrast, the epibolic movements of the **Ep**, **Er** and **El** descendants requires both cell-cell signaling based on zygotically provided factors, and neighboring clonal contacts with at least one other ectodermal clone (Fig. 10, white lines). In wild type embryos, neighbor contacts with mesodermal clones may also play a role. Thus, gastrulation can take place without any mesoderm precursor, but correct gastrulation behavior of the ectoderm cannot occur if zygotic transcription is prevented, or if more than one ectoderm precursor is missing.

This model may be tested in future studies on the molecular mechanisms directing gastrulation in *P. hawaiensis*. Separable molecular mechanisms can direct both autonomous and non-autonomous cellular processes involved in gastrulation. In *C. elegans*, actinomyosin-based contraction of ingressing cells requires only intrinsic, maternally derived cellular polarity, rather than cell-cell contacts (Lee and Goldstein, 2003). Similar signals may be operative in this amphipod, where cellular apicobasal polarity is clearly established by the holoblastic to superficial cleavage transition that takes place well before gastrulation. In *Xenopus laevis* embryos, germ layer-specific gastrulation movements occur autonomously in explants (reviewed by Keller et al., 2003). One of these movements, blastopore closure, involves the movements of ectodermal sheets of cells over the internalizing mesendoderm (Keller et al., 2003). Blastopore closure requires the activity of the planar cell polarity (PCP) pathway, including signaling through *Disheveled* (Wallingford et al., 2002). However, the requirement for *Dsh* does not extend to mesendoderm internalization or archenteron formation in *X. laevis* (Ewald et al., 2004). The PCP pathway, which is conserved in both protostomes and deuterostomes (Zallen, 2007), may thus be a promising candidate for regulation of the movements of **Ep**, **Er** and **El** during *P. hawaiensis* gastrulation.

The timing of regulative behaviors relative to gastrulation

P. hawaiensis embryos display a contrast between the regularity of the overall fate map and cell lineage, and the capacity for embryonic somatic regulation. Previous studies demonstrated that any one mesoderm precursor can replace the other two, and that loss of any one ectoderm precursor can be compensated for by one of the two remaining precursors (Price and Patel, 2008). To understand this phenomenon, we must ask at what point cells begin their regulation by responding to the absence of ablated blastomeres. We have shown that the cells comprising the mesoderm (**Mav**, **ml** and **mr**) and ectoderm (**Ep**, **Er** and **El**) equivalence groups have very different cleavage, migration and gastrulation behaviors. We might therefore expect that regulation would take place immediately following ablation. However, our lineage analyses of micromere-ablated embryos suggest that diagnostic cell cleavage and migration changes do not occur before gastrulation, setting a lower bound to the timing of regulative processes as revealed by changes in cell behavior and

morphology. The upper temporal limit to these changes is germ band formation (Price et al., 2010), delimiting a specific time window that could be the subject of future work on the molecular mechanisms of embryonic regulation.

Another question relevant to this regulation is whether it proceeds through a redeployment or reorganization of preexisting maternal factors, or through differential zygotic gene regulation. For example, in sea urchin embryos, maternally provided *vasa* transcript is normally found in all cells at the blastula stage, but Vasa protein is localized exclusively to the small micromeres. However, following micromere ablation, Vasa protein is ectopically translated in all cells, presumably from the preexisting maternal transcripts rather than as a result of *de novo* zygotic transcription (Voronina et al., 2008). In contrast, our results show that the latter mechanism is likely to operate in *P. hawaiensis* embryonic regulation, as gastrulation and lineage-specific cell behaviors proceed normally in both micromere-ablated, and transcriptionally blocked embryos.

In *C. elegans*, despite the invariant lineage patterns of wild type embryos, early cleavage cells can take on alternative cell fates under certain circumstances before, but not after, gastrulation (discussed by Yuzyuk et al., 2009). When challenged with ectopic expression of cell type-specific transcription factors (Fukushige and Krause, 2005; Gilleard and McGhee, 2001; Horner et al., 1998; Kiefer et al., 2007; Smith and Mango, 2007; Zhu et al., 1998), or moved to different embryonic positions (Priess and Thomson, 1987; Wood, 1991), early blastomeres can be induced to change fates. This provides an intriguing parallel with the capacity for somatic regulation in *P. hawaiensis* embryos. Consistent with the differentiation potential of somatic lineages being increasingly "locked in" following gastrulation, the expression of *P. hawaiensis* orthologues of the mesoderm-specific transcription factors *twist* and *mef-2* are not detected until after gastrulation (Price and Patel, 2008). The gradual loss of "developmental plasticity" in *C. elegans* is at least partially regulated by the degree of chromatin compaction via *Polycomb* complex genes (Yuzyuk et al., 2009). This suggests that chromatin, and thus gene expression, modification by the *Polycomb* complex or other global transcriptional regulators may play important roles in the ability of *P. hawaiensis* embryos to effect regulation during embryogenesis.

Supplementary materials related to this article can be found online at doi:10.1016/j.ydbio.2011.07.029.

Author contributions

FA performed experiments, analyzed data, and wrote the manuscript. BH performed experiments and analyzed data. CE proposed the idea for the research, performed experiments, analyzed data, wrote the manuscript, and obtained funding for the research. All authors read and approved the final manuscript.

Acknowledgments

Thanks to Michalis Averof, Carsten Wolff, Nikos Konstantinides, Tripti Gupta, and members of the Extavour and Akam labs for discussion of the results and comments on the manuscript, and to Marcus Bischoff and Ralf Schnabel for helpful suggestions on SIMI°BioCell. This work was partially supported by a BBSRC studentship (BH), the Harvard University Milton Fund (FA), a Seed Grant from the Harvard Stem Cell Institute (SG-0057-10-00) and an Ellison Medical Foundation Young Scholar award (AG-NS-07010-10) to CE.

References

Alwes, F., Scholtz, G., 2004. Cleavage and gastrulation of the euphausiacean *Meganyctiphanes norvegica* (Crustacea, Malacostraca). Zoomorphology 123, 125–137.

Aman, A., Piotrowski, T., 2010. Cell migration during morphogenesis. Dev. Biol. 341, 20–33.

Amma, K., 1911. Über die Differenzierung der Keimbahnzellen bei den Copepoden. Arch. Zellforsch. 6, 497–576.

Biffis, C., Alwes, F., Scholtz, G., 2009. Cleavage and gastrulation of the dendrobranchiate shrimp *Penaeus monodon* (Crustacea, Malacostraca, Decapoda). Arthropod Struct. Dev. 38, 527–540.

Bischoff, M., Parfitt, D.-E., Zernicka-Goetz, M., 2008. Formation of the embryonic-abembryonic axis of the mouse blastocyst: relationships between orientation of early cleavage divisions and pattern of symmetric/asymmetric divisions. Development 135, 953–962.

Bischoff, M., Schnabel, R., 2006. Global cell sorting is mediated by local cell-cell interactions in the *C. elegans* embryo. Dev. Biol. 294, 432–444.

Borowsky, B., 1990. Patterns of reproduction of some amphipod crustaceans and insights into the nature of their stimuli. Crustacean Sexual Biology. Columbia University Press, New York, pp. 34–49.

Browne, W.E., Price, A.L., Gerberding, M., Patel, N.H., 2005. Stages of embryonic development in the amphipod crustacean, *Parhyale hawaiensis*. Genesis 42, 124–149.

Conklin, E.G., 1905. Organization and cell lineage of the ascidian egg. J. Acad. Nat. Sci. (Philadelphia) Ser. 2 (13), 5–119.

Conlon, F., Beddington, R., 1995. Mouse gastrulation from a frog's perspective. Semin. Dev. Biol. 6, 249–256.

Deppe, U., Schierenberg, E., Cole, T., Krieg, C., Schmitt, D., Yoder, B., von Ehrenstein, G., 1978. Cell lineages of the embryo of the nematode *Caenorhabditis elegans*. Proc. Natl. Acad. Sci. U. S. A. 75, 376–380.

Dictus, W., Damen, P., 1997. Cell-lineage and clonal-contribution map of the trochophore larva of *Patella vulgata* (Mollusca). Mech. Dev. 62, 213–226.

Ewald, A.J., Peyrot, S.M., Tyszka, J.M., Fraser, S.E., Wallingford, J.B., 2004. Regional requirements for *Dishevelled* signaling during *Xenopus* gastrulation: separable effects on blastopore closure, mesendoderm internalization and archenteron formation. Development 131, 6195–6209.

Extavour, C.G., 2005. The fate of isolated blastomeres with respect to germ cell formation in the amphipod crustacean *Parhyale hawaiensis*. Dev. Biol. 277, 387–402.

Fuchs, K., 1914. Die Keimbahnentwicklung von *Cyclops viridis* JURINE. Zool. Jahr. Anat. 38, 103–156.

Fukushige, T., Krause, M., 2005. The myogenic potency of HLH-1 reveals wide-spread developmental plasticity in early *C. elegans* embryos. Development 132, 1795–1805.

Gerberding, M., Browne, W.E., Patel, N.H., 2002. Cell lineage analysis of the amphipod crustacean *Parhyale hawaiensis* reveals an early restriction of cell fates. Development 129, 5789–5801.

Gilleard, J.S., McGhee, J.D., 2001. Activation of hypodermal differentiation in the *Caenorhabditis elegans* embryo by GATA transcription factors ELT-1 and ELT-3. Mol. Cell. Biol. 21, 2533–2544.

Hejnol, A., Schnabel, R., 2006. What a couple of dimensions can do for you: comparative developmental studies using 4D microscopy-examples from tardigrade development. Integr. Comp. Biol. 1–11.

Hertzler, P.L., Clark Jr., W.H., 1992. Cleavage and gastrulation in the shrimp *Sicyonia ingentis*: invagination is accompanied by oriented cell division. Development 116, 127–140.

Hertzler, P.L., Wang, S.W., Clark Jr., W.H., 1994. Mesendoderm cell and archenteron formation in isolated blastomeres from the shrimp *Sicyonia ingentis*. Dev. Biol. 164, 333–344.

Horner, M.A., Quintin, S., Domeier, M.E., Kimble, J., Labouesse, M., Mango, S.E., 1998. pha-4, an HNF-3 homolog, specifies pharyngeal organ identity in *Caenorhabditis elegans*. Genes Dev. 12, 1947–1952.

Ip, Y.T., Maggert, K., Levine, M., 1994. Uncoupling gastrulation and mesoderm differentiation in the *Drosophila* embryo. EMBO J. 13, 5826–5834.

Jacob, S.T., Sajdel, E.M., Munro, H.N., 1970. Specific action of alpha-amanitin on mammalian RNA polymerase protein. Nature 225, 60–62.

Keller, R., Davidson, L.A., Shook, D.R., 2003. How we are shaped: the biomechanics of gastrulation. Differentiation 71, 171–205.

Kiefer, J.C., Smith, P.A., Mango, S.E., 2007. PHA-4/FoxA cooperates with TAM-1/TRIM to regulate cell fate restriction in the *C. elegans* foregut. Dev. Biol. 303, 611–624.

Klag, J., Swiatek, P., 1999. Differentiation of primordial germ cells during embryogenesis of *Allacma fusca* (L.) (Collembola: Symphypleona). Int. J. Insect Morphol. Embryol. 28, 161–168.

Kühn, A., 1908. Die Entwicklung der Keimzellen in den parthenogenetischen Generationen der Cladoceren *Daphnia pulex* DE GEER und *Polyphemus pediculus* DE GEER. Arch. Zellforsch. 1, 538–586.

Kühn, A., 1911. Über determinierte Entwicklung bei Cladoceren. Zool. Anz. 38, 345–357.

Langenbeck, C., 1898. Formation of the germ layers in the amphipod *Microdeutopus gryllotalpa* Costa. J. Morphol. 14, 301–336.

Lee, J.Y., Goldstein, B., 2003. Mechanisms of cell positioning during *C. elegans* gastrulation. Development 130, 307–320.

Leptin, M., 1999. Gastrulation in *Drosophila*: the logic and the cellular mechanisms. EMBO J. 18, 3187–3192.

Leptin, M., Grunewald, B., 1990. Cell shape changes during gastrulation in *Drosophila*. Development 110, 73–84.

Liu, H., Kim, J.M., Aoki, F., 2004. Regulation of histone H3 lysine 9 methylation in oocytes and early pre-implantation embryos. Development 131, 2269–2280.

McMahon, A., Reeves, G.T., Supatto, W., Stathopoulos, A., 2010. Mesoderm migration in *Drosophila* is a multi-step process requiring FGF signaling and integrin activity. Development 137, 2167–2175.

Nance, J., Lee, J.-Y., Goldstein, B., 2005. Gastrulation in *C. elegans*. WormBook: The Online Review of *C. elegans* Biology, pp. 1–13.
Newport, J., Kirschner, M., 1982. A major developmental transition in early *Xenopus* embryos: I. characterization and timing of cellular changes at the midblastula stage. Cell 30, 675–686.
Nishida, H., Satoh, N., 1983. Cell lineage analysis in ascidian embryos by intracellular injection of a tracer enzyme: I. Up to the eight-cell stage. Dev. Biol. 99, 382–394.
Patel, H.N., Martin-Blanco, E., Coleman, K.G., Poole, S.J., Ellis, M.C., Kornberg, T.B., Goodman, C.S., 1989. Expression of *engrailed* proteins in arthropods, annelids, and chordates. Cell 58, 955–968.
Patel, N.H., 1994. Imaging neuronal subsets and other cell types in whole-mount *Drosophila* embryos and larvae using antibody probes. Methods in Cell Biology, 44. Academic Press, Inc., pp. 445–487.
Pawlak, J.B., Sellars, M.J., Wood, A., Hertzler, P.L., 2010. Cleavage and gastrulation in the Kuruma shrimp *Penaeus (Marsupenaeus) japonicus* (Bate): a revised cell lineage and identification of a presumptive germ cell marker. Dev. Growth Differ. 52, 677–692.
Poulson, D.F., 1947. The pole cells of Diptera, their fate and significance. Proc. Natl. Acad. Sci. U. S. A. 182–184.
Price, A.L., Gastrulation and Mesodem Development in *Parhyale hawaiensis*. Committee on Developmental Biology, Vol. Ph. D. University of Chicago, Chicago, 2005, pp. 199.
Price, A.L., Modrell, M.S., Hannibal, R.L., Patel, N.H., 2010. Mesoderm and ectoderm lineages in the crustacean *Parhyale hawaiensis* display intra-germ layer compensation. Dev. Biol. 341, 256–266.
Price, A.L., Patel, N.H., 2008. Investigating divergent mechanisms of mesoderm development in arthropods: the expression of *Ph-twist* and *Ph-mef2* in *Parhyale hawaiensis*. J. Exp. Zool. B Mol. Dev. Evol. 310, 24–40.
Priess, J.R., Thomson, J.N., 1987. Cellular interactions in early *C. elegans* embryos. Cell 48, 241–250.
Rehm, E.J., Hannibal, R.L., Chaw, R.C., Vargas-Vila, M.A., Patel, N.H., 2008. The crustacean *Parhyale hawaiensis*, a new model for arthropod development. Emerging Model Organisms: A Laboratory Manual, vol. 1. CSHL Press, Cold Spring Harbor, pp. 373–404.
Schnabel, R., Hutter, H., Moerman, D., Schnabel, H., 1997. Assessing normal embryogenesis in *Caenorhabditis elegans* using a 4D microscope: variability of development and regional specification. Dev. Biol. 184, 234–265.
Scholtz, G., Wolff, C., 2002. Cleavage, gastrulation, and germ disc formation of the amphipod *Orchestia cavimana* (Crustacea, Malacostraca, Peracarida). Contrib. Zool. 71, 9–28.
Simpson, P., 1983. Maternal–zygotic gene interactions during formation of the dorsoventral pattern in *Drosophila* embryos. Genetics 105, 615–632.
Skiba, F., Schierenberg, E., 1992. Cell lineages, developmental timing, and spatial pattern formation in embryos of free-living soil nematodes. Dev. Biol. 151, 597–610.
Smith, P.A., Mango, S.E., 2007. Role of T-box gene tbx-2 for anterior foregut muscle development in *C. elegans*. Dev. Biol. 302, 25–39.
Stern, C.D. (Ed.), 2004. Gastrulation: From Cells to Embryo. Cold Spring Harbor Laboratory Press, Cold Spring Harbor, NY.
Sulston, J.E., Schierenberg, E., White, J.G., Thomson, J.N., 1983. The embryonic cell lineage of the nematode *Caenorhabditis elegans*. Dev. Biol. 100, 64–119.
Tam, P.P., Williams, E.A., Chan, W.Y., 1993. Gastrulation in the mouse embryo: ultrastructural and molecular aspects of germ layer morphogenesis. Microsc. Res. Tech. 26, 301–328.
Tassy, O., Daian, F., Hudson, C., Bertrand, V., Lemaire, P., 2006. A quantitative approach to the study of cell shapes and interactions during early chordate embryogenesis. Curr. Biol. 16, 345–358.
Taube, E., 1909. Beiträge zur Entwicklungsgeschichte der Euphausiden. Z. Wiss. Zool. 92, 427–464.
van den Biggelaar, J.A., Dictus, W.J., van Loon, A.E., 1997. Cleavage patterns, cell-lineages and cell specification are clues to phyletic lineages in Spiralia. Semin. Cell Dev. Biol. 8, 367–378.
Voronina, E., Lopez, M., Juliano, C.E., Gustafson, E., Song, J.L., Extavour, C.G., Casella, S.G., Oliveri, P., McClay, D., Wessel, G., 2008. Vasa protein expression is restricted to the small micromeres of the sea urchin, but is inducible in other lineages early in development. Dev. Biol. 314, 276–286.
Wallingford, J.B., Fraser, S.E., Harland, R.M., 2002. Convergent extension: the molecular control of polarized cell movement during embryonic development. Dev. Cell 2, 695–706.
Wang, S.W., Hertzler, P.L., Clark Jr., W.H., 2008. Mesendoderm cells induce oriented cell division and invagination in the marine shrimp *Sicyonia ingentis*. Dev. Biol. 320, 175–184.
Wolff, C., Scholtz, G., 2002. Cell lineage, axis formation, and the origin of germ layers in the amphipod crustacean *Orchestia cavimana*. Dev. Biol. 250, 44–58.
Wood, W.B., 1991. Evidence from reversal of handedness in *C. elegans* embryos for early cell interactions determining cell fates. Nature 349, 536–538.
Yin, C., Ciruna, B., Solnica-Krezel, L., Thomas, L., 2009. Chapter 7 Convergence and extension movements during vertebrate gastrulation. Current Topics in Developmental Biology, vol. 89. Academic Press, pp. 163–192.
Yuzyuk, T., Fakhouri, T.H.I., Kiefer, J., Mango, S.E., 2009. The polycomb complex protein mes-2/E(z) promotes the transition from developmental plasticity to differentiation in *C. elegans* embryos. Dev. Cell 16, 699–710.
Zallen, J.A., 2007. Planar polarity and tissue morphogenesis. Cell 129, 1051–1063.
Zhu, J., Fukushige, T., McGhee, J.D., Rothman, J.H., 1998. Reprogramming of early embryonic blastomeres into endodermal progenitors by a *Caenorhabditis elegans* GATA factor. Genes Dev. 12, 3809–3814.

Supplementary Material for

Patterns of cell lineage, movement, and migration from germ layer specification to gastrulation in the amphipod crustacean *Parhyale hawaiensis*.
Alwes, F., Hinchen, B. and **Extavour, C G.**, *Developmental Biology* 359(1): 110-123 (2011)

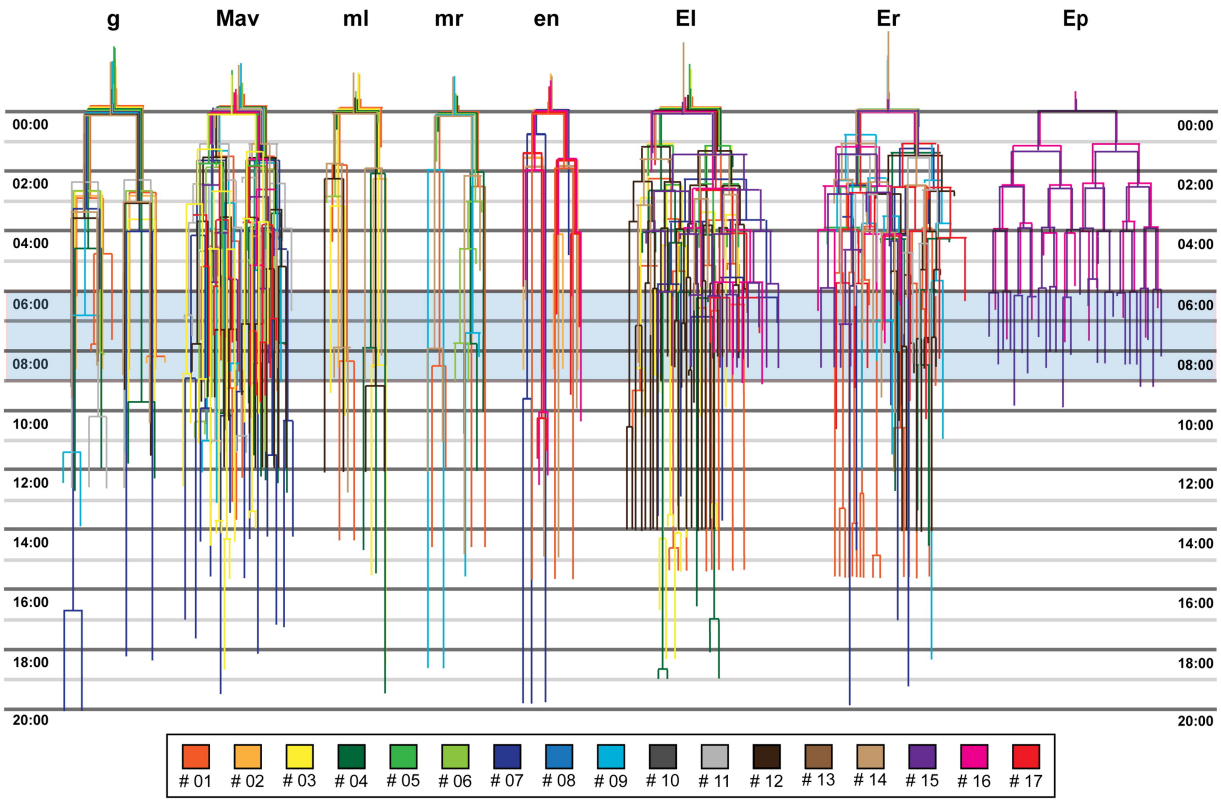

Supplementary Fig. 1. Superimposed lineage trees for individual embryos. Lineage patterns for individual third cleavage blastomeres are superimposed and normalized to the same starting time (00:00 indicates fourth cleavage). Blue shading indicates the time at which embryos reach the rosette stage. Legend: each embryo that was analyzed with SIMI°BioCell (see Table 1) is indicated with a different color.

Supplementary Movie S1. The early development of two *P. hawaiensis* embryos shown from the eight-cell stage until the onset of gastrulation. The embryo on the right shows a view of **g**, **Mav**, **ml**, and **El**. In this embryo the formation of the rosette and subsequent gastrulation are visible. The embryo on the left shows a view of **en**, **Ep**, **mr**, and **Er**. In this view the movement of cells towards the rosette on the one hand (**mr**) and towards the forming germ disk (**Ep** and **Er**) can be followed up to the rosette stage. The red and green dots appearing in the left embryo are the original labeling of cell lineages using SIMI°BioCell. The temporarily disappearing dots are caused by program settings.

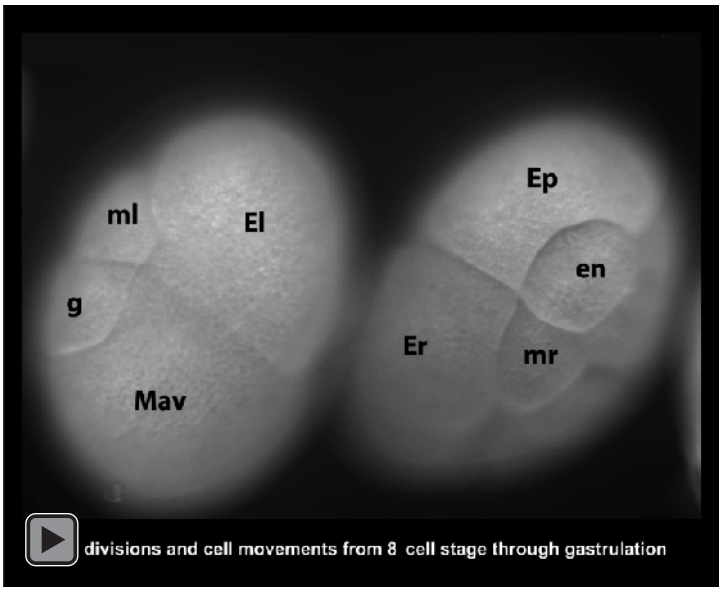

Supplementary Movie S2. Cell morphological changes during early development until the onset of gastrulation. The embryos on the right show a view of the micromeres **g**, **ml**, **mr**, and **en**. The embryo on the left is slightly rotated towards **Mav** so that the region of the future rosette is visible. The green and red dots generated by SIMI°BioCell mark the cell lineage of **g**, with the red dot specifically marking the lineage of the **g** descendant that ingresses first during rosette formation. The appearance of cell morphological changes are annotated for selected cells throughout the movie.